# SEISMIC DATA PROCESSING REPORT

## Geological Survey of Western Australia
## Mid-West 1 and 2 Deep Crustal 2D

## 23GSWA-MW1 and 23GSWA-MW2

| | |
|---|---|
| REV, DATE | REV2, 30 JULY 2024 |
| PREPARED BY | REECE CUNNOLD, JENNIFER ALLEN, SASHA ZIRAMOV |
| REVIEWED BY | GREG TURNER |

# EXECUTIVE SUMMARY

HiSeis conducted the acquisition and processing of deep crustal, 2D seismic reflection data for the Geological Survey of Western Australia (GSWA). The project involved 2 lines, the 352 km-long line, 23GSWA-MW1, spanning from Mt Magnet to Geraldton along sealed gazetted roads and the 190k km-long line, 23GSWA-MW2, spanning from 20 km east of Latham township to Greenhead. Data collection for MW1 began on 28/11/23 and concluded on 19/12/23. Data collection for MW2 began on 11/01/24 and concluded on 21/01/24. The eastern end of 23GSWA-MW1 overlaps with the line 10GA-YU3 from a previous deep crustal vintage.

Data was recorded using Quantum 5Hz geophone receiver nodes positioned at 10m intervals, extending up to 30km from the source (nominal ±8km). Three 60,000 lb Vibroseis source vehicles generated seismic energy at 40m intervals with a 24-second sweep from 3 - 96Hz.

Data processing commenced in January 2024. A custom workflow was developed, specifically tailored to the acquisition parameters, survey objectives, and current geological understanding. Following a thorough initial data quality control step, a comprehensive first-break picking program was implemented to precisely define the first arrival wavefront. To enhance the depth penetration of the resulting refraction tomography velocity model, the contracted maximum offset for first-break picking was extended from 1.5 km to 3 km.

Data preprocessing addressed noise sources, primarily traffic-related, through attenuation techniques and signal enhancement. Static corrections were applied using final datums of 460 metres for MW1 and 370 metres for MW2, both using a replacement velocity of 5,800 m/s. Velocity analysis was conducted iteratively before implementing the final Kirchoff Pre-Stack Time Migration (PreSTM). The migrated gathers underwent further conditioning and were stacked to generate two final subsurface images focused on shallow and deep targets, respectively. These images revealed notable features along the entire seismic line, including the geometry of the Perth Basin, the continuity and character of major faults, such as the Darling Fault, and the crustal architecture of the Yilgarn Craton.

Three iterations of reflection tomography were undertaken to generate an interval velocity model in depth. For each iteration this involved sparsely migrating the data and picking residual moveout. The updated velocity model was compared against well logs where available. The final Pre-Stack Depth migrated product showed significant uplift at line bends and areas of sharp lateral velocity contrast, particularly near the Darling Scarp and through the Perth Basin.

Some recommendations are made for future seismic surveys.

1. Resampling for Improved Efficiency: These regional seismic lines represent large datasets due to their length, high trace density, long record length, and 2ms sample rate. While the 2ms sample rate was maintained throughout processing, the maximum sweep frequency used was only 96Hz. In such cases, resampling the data to 4ms can significantly improve processing runtimes and reduce disk space requirements by half. This resampling would not degrade the seismic bandwidth or resolution as the highest recoverable frequency content is well below the Nyquist frequency defined by the original 2ms sample rate. Implementing this approach in future surveys with similar acquisition parameters would enhance processing efficiency without compromising data quality.

2. Targeted Infill Shooting: The infill shots acquired on either side of exclusion zones where seismic acquisition was not permitted appear to have limited impact on image quality within

those gaps. These additional shots could have been more strategically deployed within the Perth Basin where several lines exhibit consistently lower reflectivity. Future surveys in the Perth Basin might benefit from utilizing multiple sweeps on each station and vertically summing the recorded data to potentially improve data quality and subsurface imaging.

# Contents

## LIST OF FIGURES

## LIST OF TABLES

# 1 INTRODUCTION

## 1.1 BACKGROUND

HiSeis was contracted to acquire and process deep crustal, 2D seismic reflection data on behalf of the Geological Survey of Western Australia (GSWA) in the Southwest and Midwest Regions of Western Australia as part of the Western Australia Exploration Incentive Scheme (EIS). The final 2D lines, named 23GSWA-MW1 (Figure 1) and 23GSWA-MW2 (Figure 2), covered approximately 352 km and 190 km respectively of sealed gazetted roads. 23GSWA-MW1 started in Mt Magnet in November 2023 and finished in Geraldton on 19 December 2023. 23GSWA-MW2 started 20 km from Latham township in January 2024 and finished in Greenhead on 21 January 2024. With Both lines starting in the east, surface elevation varies from 456m to sea-level for MW1 and 364m to sea-level for MW2 (Figure 3 and Figure 4).

In the east the 23GSWA-MW1 line intersects with the 10GA-YU lines from a previous deep crustal vintage. Moving west both lines extend over the western Yilgarn Craton, covering the Youanmi Terrane, and the Perth Basin

Seismic data processing was conducted in Perth, Australia by HiSeis between January 2024 and July 2024.

## 1.2 OBJECTIVES

GSWA identified the following survey objectives.

- Imaging the deep crustal architecture of the survey area.
- Identify the structure, geometry, and relationship between various geological domains.
- Image from the surface to below the Moho.


Figure 1. 23GSWA-MW1 Location map

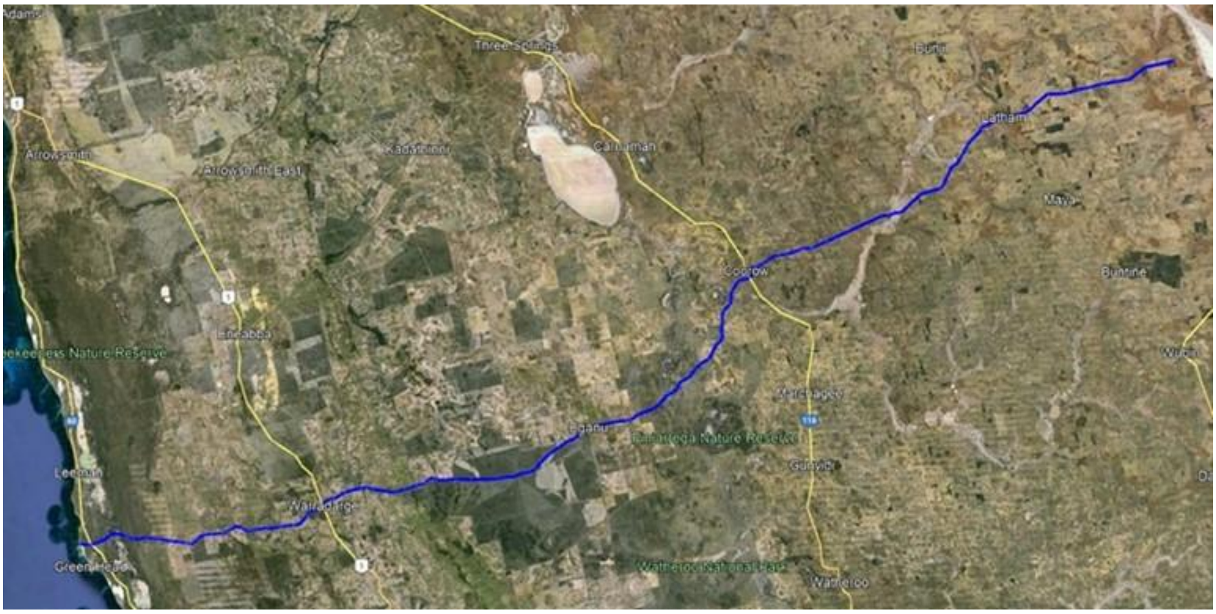


Figure 2. 23GSWA-MW2 Location map

# 2 ACQUISITION

Data was recorded using Quantum 5Hz geophone receiver nodes, spaced at 10m intervals along the nominal active split spread of +-8k. However, many more nodes were deployed beyond the nominal spread and all remained active offering maximum offsets out to approximately 30km, resulting in a maximum CDP fold of 549 (MW1), and 555 (MW2). An inline array of three 60,000 lb Vibroseis source vehicles produced seismic energy, delivering a 24 second sweep through a frequency range of 3 - 96Hz. The nominal source spacing along each line was 40m co-located with receiver stations. Infill/make-up shots were taken at half the nominal source interval when approaching exclusion zones. The source/receiver line is marked blue in Figure 1, and Figure 2 above.

Detailed acquisition parameters are presented in Table 1. The Vibroseis sweep definition is outlined in Table 2. A map of source and receiver elevations are shown in Figure 3, and Figure 4.

Table 1. MW1 and MW2 acquisition parameters

| **2D Acquisition Parameters** | |
|---|---|
| Total Survey Length | 2 lines; 351.98km (MW1), 189.64km (MW2) |
| Receiver Type | Quantum PS-5GR 5Hz geophone |
| Number of Receiver Stations | 34629 (MW1); 18564 (MW2) |
| Active Receiver Spread (maximum) | Nominal +- 8km split spread, all live with additional receivers being deployed and retrieved. |
| Receiver station spacing | 10m |
| Total Number of Source Stations | 8955 (MW1); 4705 (MW2) |
| Source Station Spacing | 40m nominal with 20m infill around gaps |
| Max Fold | 549 (MW1), 555 (MW2) using all offset |
| Offset | +-8000m nominal, 29996m (MW1), 30263m (MW2) max |
| Record length | 20sec |
| Sample interval | 2ms |
| Coordinate reference system | GDA2020, MGA Zone 50 |

Table 2: MW1 and MW2 sweep parameters.

| Standard Sweep Definition MW1 and MW2 | |
|---|---|
| Vibrators | INOVA AHV-IV 60, 000 lb |
| Electronics | INOVA VibPro HD |
| Sweep Frequency Range | 3 – 96 Hz |
| Sweep Duration | 24 second nominal |
| Sweep Type | Weibull base |
| Tapers | 500ms in, 600ms out |
| Vibrator Array | 3 vibrators inline configuration |
| Operating Force | 70% |
| Phase Locking | Ground force |
| Amplitude Control | Peak-to-peak |

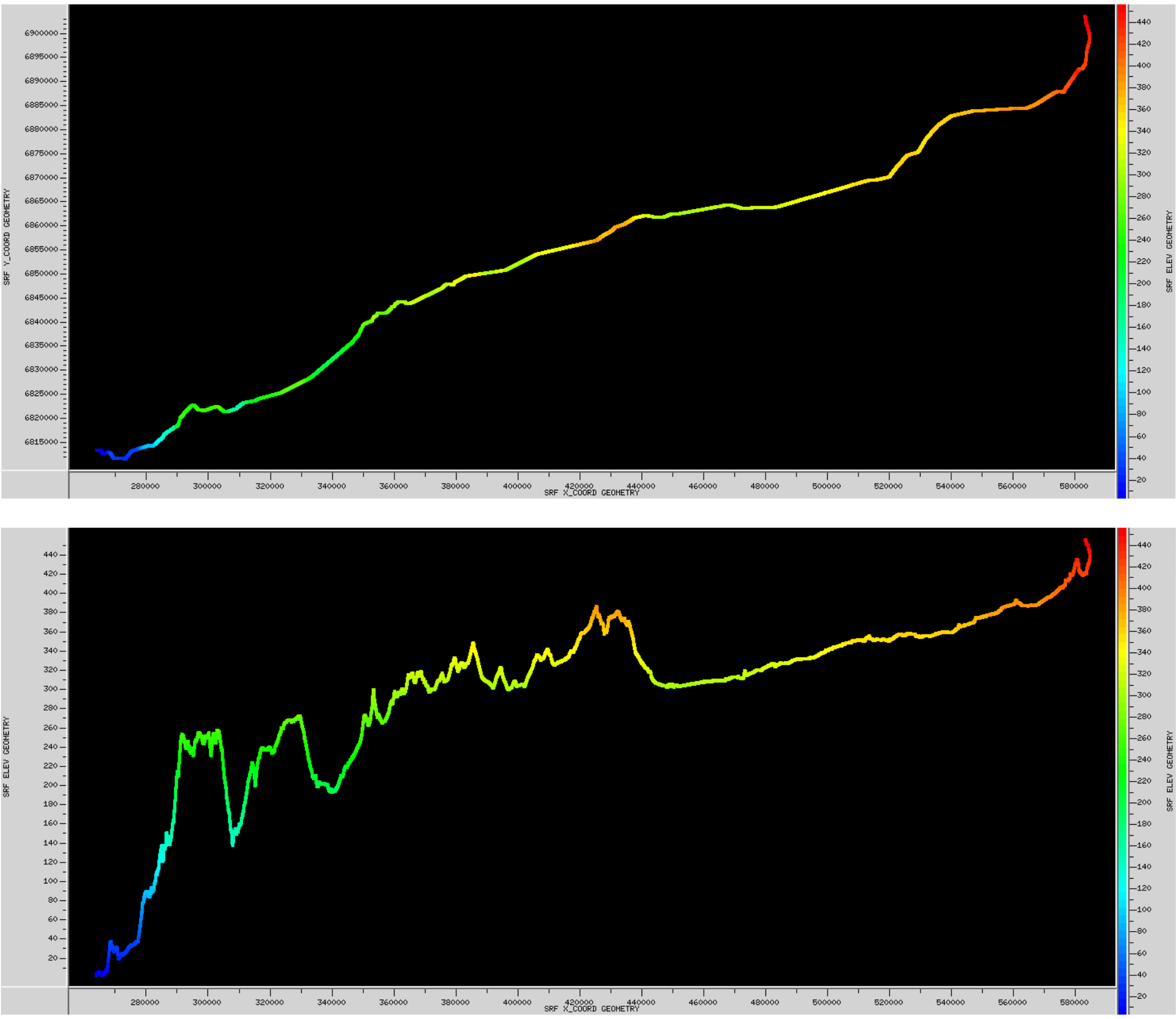


Figure 3. MW1 Elevation map (top) and profile (bottom)

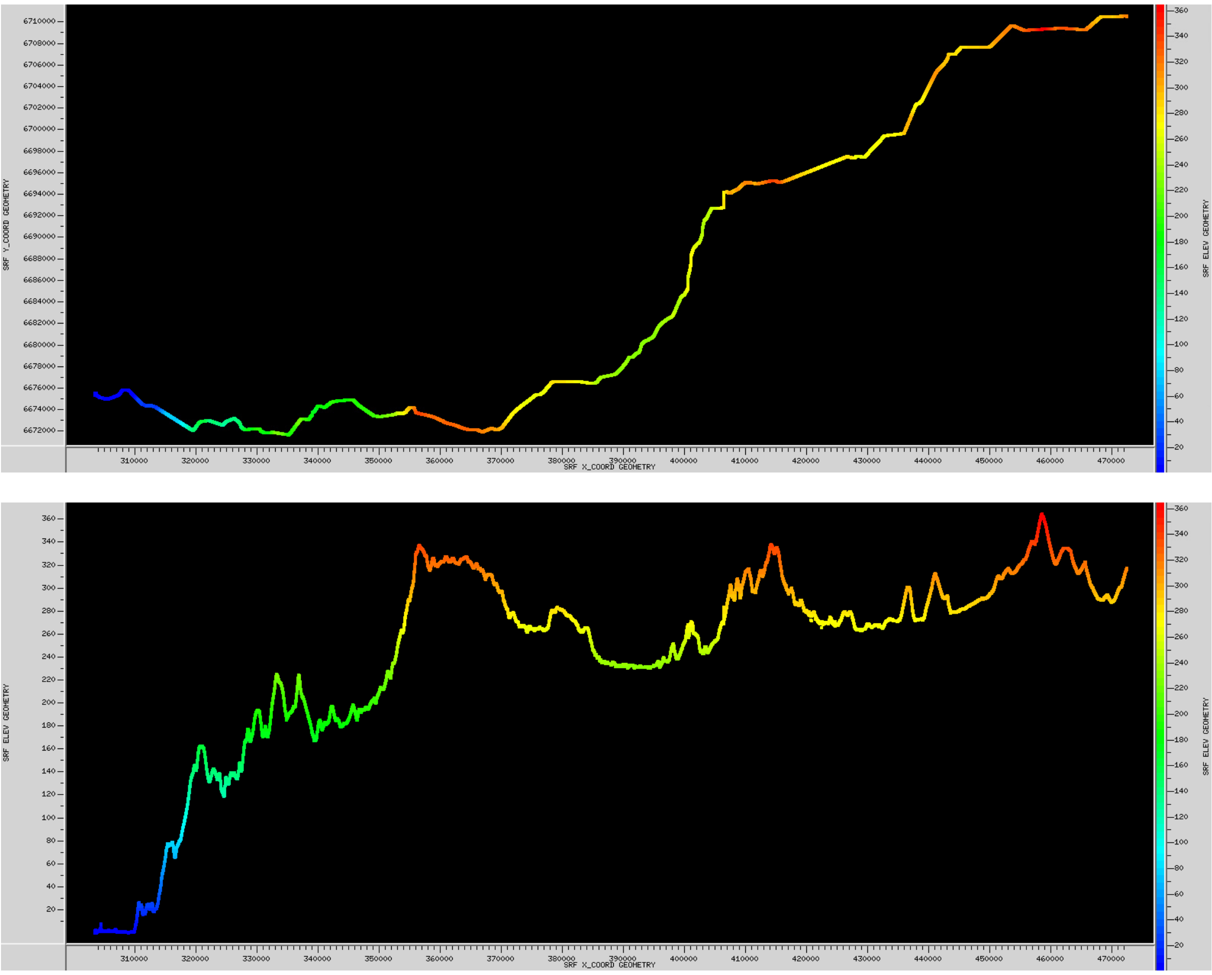


Figure 4. MW2 Elevation map (top) and profile (bottom)

In Figure 3 and Figure 4 (above), the top image shows the receiver X and Y coordinate with the 2D line coloured by elevation. The bottom image shows the elevation profile with the receiver position on the X-axis and elevation on the Y-axis.

Below, in Figure 5 and Figure 6, the fold of the survey is shown using the CDP X and Y coordinates and the 2D line coloured by fold. The fold map includes all active receivers. Maximum fold is 549 for MW1 and 555 for MW2.

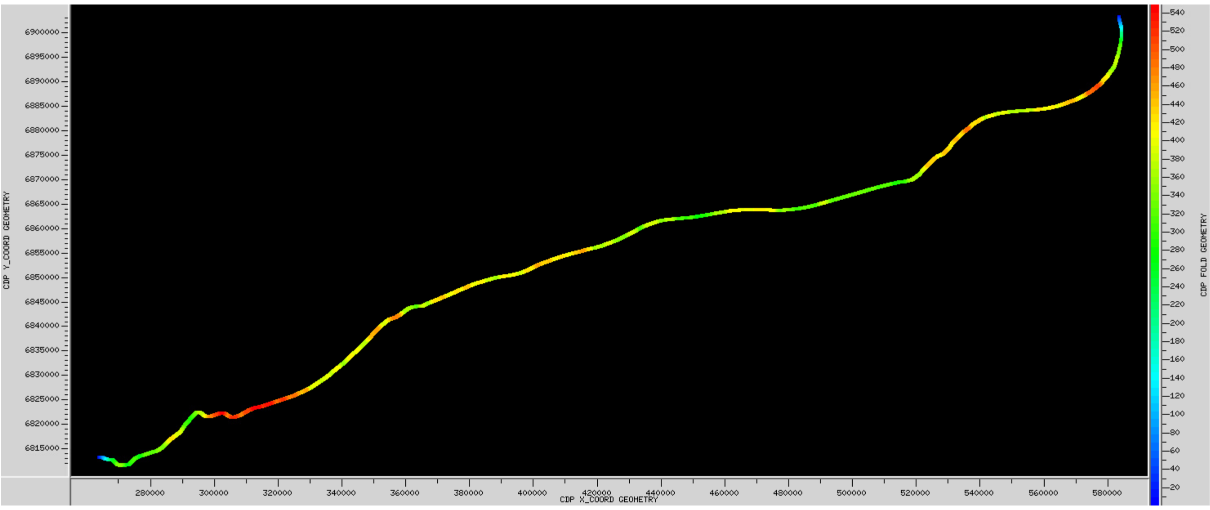


Figure 5. MW1 CDP Fold map

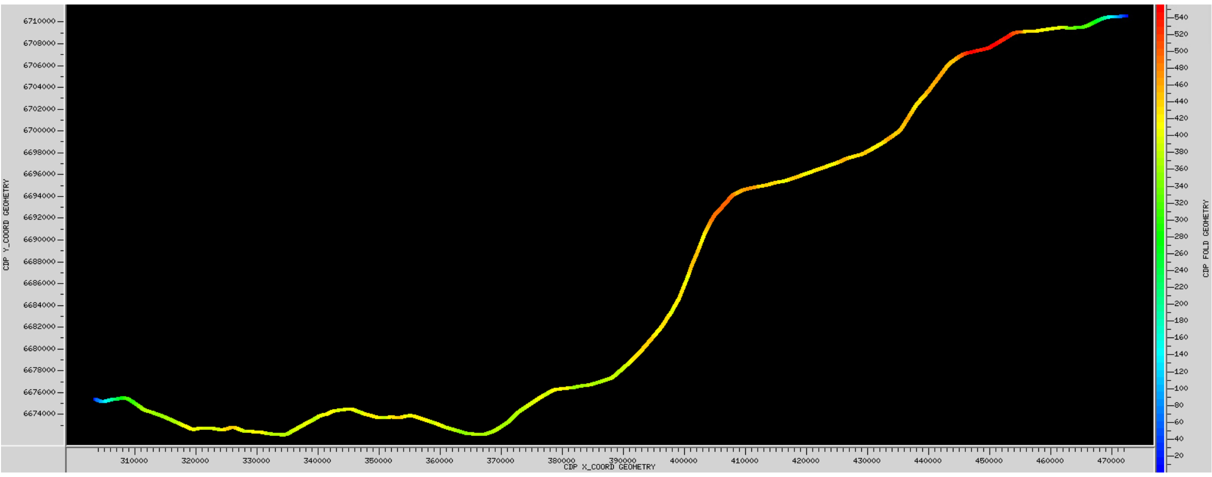


Figure 6. MW2 CDP Fold map

# 3 PROCESSING

## 3.1 OVERVIEW

The processing flow included refraction tomography, comprehensive pre-processing and noise attenuation processes, several iterations of velocity analysis and Pre-stack Time Migration. The pre-processed gathers were also used to perform 3 iterations of reflection tomography to update the velocity model prior to producing a final Pre-stack Depth Migrated product as explained in section 4.

Final datums of 460m (MW1) and 370m (MW2), with a replacement velocity of 5800m/s were selected for the Pre-Stack Time Migration flow so all data would lie below the final datum. Pre-Stack Depth Migration was run from topography.

Testing was generally performed on a subset of shot gathers evenly spaced along the line with an interval of 5000 (MW1), and 2000 (MW2) stations. However, at locations such as the Darling Scarp and Perth Basin a denser QC was undertaken as required. Results from testing were presented during weekly meetings with GSWA for production approval. Presentations from weekly meetings are listed in appendix 8.4**.**

Table 3. Processed data parameters

| **Processed data parameters** | |
|---|---|
| Processed record length | PreSTM: 20sec/50km and 8sec/26km<br>PreSDM: 50km |
| Processed sample rate | Time:2ms<br>Depth: 4m |
| Final datum | 460 m (MW1); 370m (MW2) |
| Replacement velocity | 5800 m/s |
| Coordinate reference system | GDA 2020, MGA zone 50 |
| Phase | Zero phase |
| Polarity | SEG positive. An increase in acoustic impedance is a peak |

## 3.2 PROCESSING FLOW

Table 4. 2D processing flow.

| 2D Processing Flow |
|---|
| 1. SEGY input: 20000ms @ 2ms |
| 2. Geometry assignment: CDP spacing of 5m<br>Offset binning 50m – 10050m (100m)<br>Manual picking of CDP track close to receiver line |
| 3. First break picking of every shot out to 3km offset |
| 4. Refraction tomography & refraction static computation<br>Final datum 460m (MW1); 370m (MW1), replacement velocity 5800 m/s |
| 5. Quality control of the refraction static solution (on shot records, every 100$^{th}$ shot) |
| 6. Trace kill dead/weak traces |
| 7. Amplitude balance: $T^{1.1}$ and $Offset^{1.1}$, wrapped around processes 8 to 14 as required. |
| 8. TFDN common channel domain (MW1 only): 3-250Hz, 7 traces, 250ms |
| 9. Apply refraction statics to floating datum |
| 10. Deconvolution:<br>Zero phase spike,<br>1.5s window, 100ms operator, 1% pre-whitening |
| 11. Air blast attenuation: 345 m/s (MW1); 345m/s, 350m/s, and 355m/s (MW2) |
| 12. Surface wave noise attenuation: 100ms wrap-around AGC<br>Hard rock: 2800m/s, 3-80Hz<br>Basin: 1200m/s (MW1),1000m/s (MW2) 3-80Hz |
| 13. TFDN shot domain (MW1 only): 0-125Hz, 5 traces, 500ms, 0-1500ms |
| 14. TFDN common channel domain (MW2 only): 0-250Hz, 5 traces |
| 15. Dip Filter (MW2 only): 75 max offset<br>2-4-90-100Hz<br>1000-1200-3400-3600m/s and 200-300-900-1000m/s |
| 16. Constant velocity stack analysis for velocity guide function |
| 17. Residual statics:<br>4sec window centred on 3000ms<br>11 CDP smash to form pilot trace |
| 18. 1$^{st}$ Pass IVA on conditioned, pre-migration, super-gathers at 5km intervals. |
| 19. Pre-Stack Time Migration for velocity analysis:<br>0-8000ms @4ms<br>Every 5$^{th}$ CDP<br>Offset binning 50m - 10050m x 100m<br>75deg dip limit, 30km aperture |
| 20. 2$^{nd}$ pass IVA picked at 2km intervals |

21. Pre-Stack Time Migration for velocity analysis:
    0-20000ms @ 4ms
    Every 5th CDP
    Offset binning 50m - 10050m x 100m
    75deg dip limit, 30km aperture

22. 3rd pass IVA picked at 1km intervals.

23. Amplitude recovery for final migration: 4000ms AGC and, remove $T^{1.1}$

24. Shift to final datum 460m (MW1 only)

25. Final PreSTM:
    0-20000ms @ 2ms
    5m CMP spacing,
    Offset binning 50m-10050m x 100m,
    75deg dip limit, 30km aperture

26. Linear noise attenuation: 100ms wrap-around AGC
    5000m/s dip
    100m trace spacing.
    0-120 Hz

27. High density velocity analysis: QC at 500m intervals and pick as required.

28. Post migration amplitude balance:
    8 second dataset: 500ms AGC
    20 second dataset: 3000ms AGC

29. Trace mute:
    8 second dataset: Near 0-15 degrees
    Mid 15-30 degrees
    Far 30-45 degrees
    Full hand-picked (50deg approx.)

    20 second dataset: 2deg inner, hand-picked outer

30. Stack using 1/n

31. Shift to final datum 370m (MW2 only)

32. Random noise attenuation: F-X deconvolution
    31 traces
    10% white noise
    750ms window
    0-250 Hz

33. Time-varying bandpass filter
    CDP 220000:10-20-80-100, 0-300ms; 4-8-80-100, 400-20000ms
    CDP 271000:10-20-80-100, 0-300ms; 4-8-80-100, 400-20000ms
    CDP 273000:2-4-80-100, 0-300ms; 2-4-80-100, 400-20000ms
    CDP 281000:10-20-80-100, 0-300ms; 4-8-80-100, 400-20000ms
    CDP 289254:10-20-80-100, 0-300ms; 4-8-80-100, 400-20000ms

34. Time-varying gain: 8 second dataset only, -8dB/s @ 0-1000ms

35. Coherence filter:
 8 second dataset: 21 traces
 ±7ms/trace

 20 second dataset: 21 traces
 ±9ms/trace

36. Post-stack amplitude balance: 20 second dataset only, record length AGC

37. Time/depth conversion using smoothed migration velocity

38. Output data to SEGY

## 3.3 DATA PREPARATION & QC

Data quality was monitored daily during acquisition with ongoing uploads of receiver gathers from the field to the office for visual inspection and geometry QC. Upon completion of acquisition shot gathers were transcribed in SEGY format and returned to the Perth office along with the observer logs and survey information for further QC and processing.

Shot and receiver peg coordinates and relational information data were cross-checked throughout loading and geometry assignment. The geometry was verified by overlaying a theoretical airwave and refractor velocities on the raw data. Figure 7 shows the header overlay for shot QC performed on the 15/12/23.

Noise QC plots were generated during field QC as seen in Figure 8. These plots are derived using the signal-to-noise ratio over a window. Typical sources of noise were vehicles travelling on the road, stationary infrastructure, and wind.

Elevation measurements were compared between source stations and the surveyed receiver stations. Some discrepancies in the recorded source elevations were observed. Given the near coincident source and receiver positions, these discrepancies were corrected using a bulk shift to align with the receiver elevations.

Rigorous first break picking was carried out using a combination of manual and automated picking methods for every record. HiSeis was contracted to pick first breaks out to a maximum offset of 1500m. However, given the high data quality and ease of picking HiSeis extended the picking out to 3km to provide a better velocity model from refraction tomography and a better refraction statics solution.

Data was binned with a nominal 5m trace spacing. Given the crookedness of the line, the crossline offset of the nominal CDP track (as defined by the processing software) was significant and would cause gaps and artefacts in the stack data. To minimise these gaps and artefacts a CDP track was manually picked following closer to the receiver line and a 51-point smoother was applied. Offset binning was performed using 50m – 10050m x 100m.

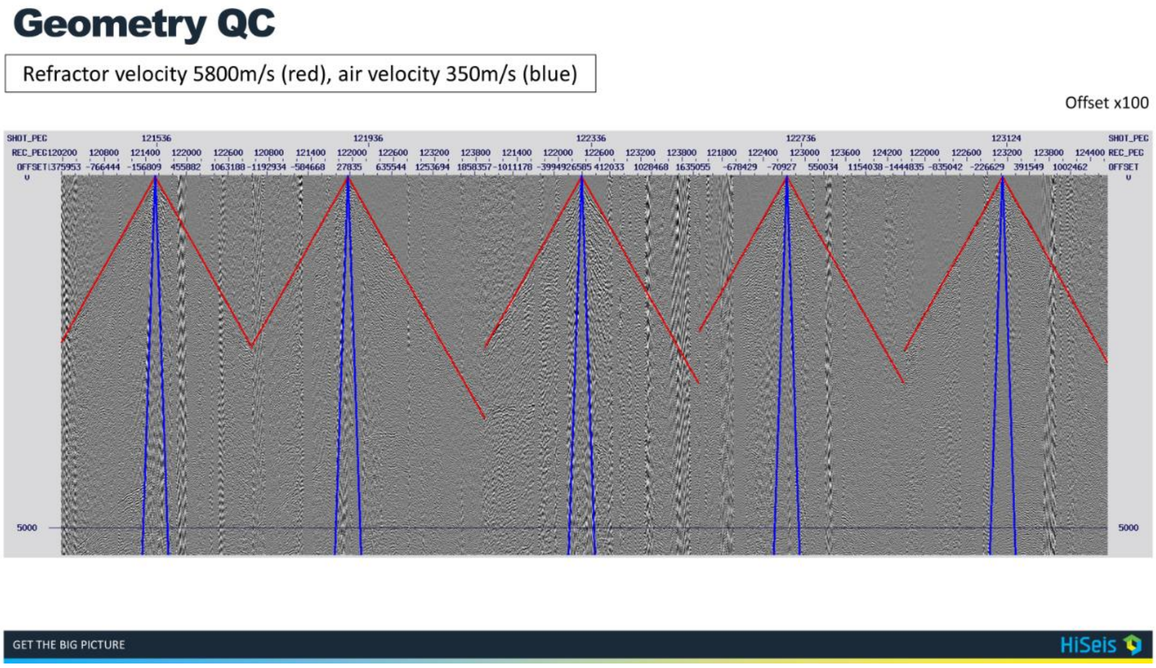


Figure 7. 2D Line raw shot gather air blast (blue), refractor (red)

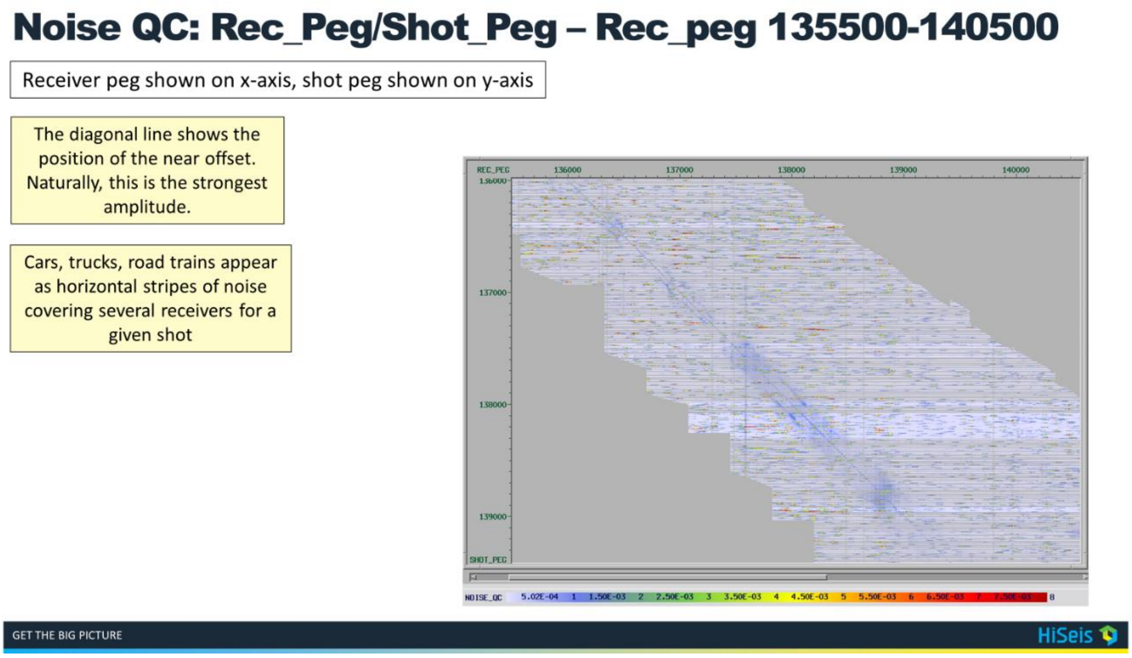


Figure 8. Example noise QC plot

## 3.4 REFRACTION TOMOGRAPHY

Rigorous first break picking, and high-resolution refraction tomography was used to generate a velocity model, ray-path model and extracted iso-velocity surfaces. These attributes provide excellent near-surface geological information and may be used to estimate the depth to the top of fresh rock as well as identify any features that may imprint on this contact. The velocity model may also be used in the calculation of refraction statics.

The refraction tomography inversion process ray traces synthetic travel times for each shot such that the difference between the input first breaks picks and synthetic first breaks are minimised. By comparing estimated and known travel times, the velocity of the medium through which the rays travelled can be iteratively deduced. As the computation is based on refracted energy, the model is accurate to the top of the deepest refractor where adequate ray coverage exists.

The velocity models for 23GSWA-MW1 and 23GSWA-MW2 (Figure 9 and Figure 12) appear well defined with strong ray penetration through the weathering layers over the Yilgarn and Youanmi Terrane. In the Perth Basin the shallow velocity is defined to ~1.5km. However, the depth to basement cannot be determined as rays (Figure 10 and Figure 13) do not penetrate deep enough with the 3km absolute offset first break picking limit. The velocity can only be defined down to the deepest ray-paths as seen in Figure 10 and Figure 13, below this the velocity is extrapolated to the bottom of the image.

Due to the length of the line please note the very large vertical exaggeration on Figure 9, Figure 10, Figure 11, Figure 12, Figure 13. and Figure 14 below.

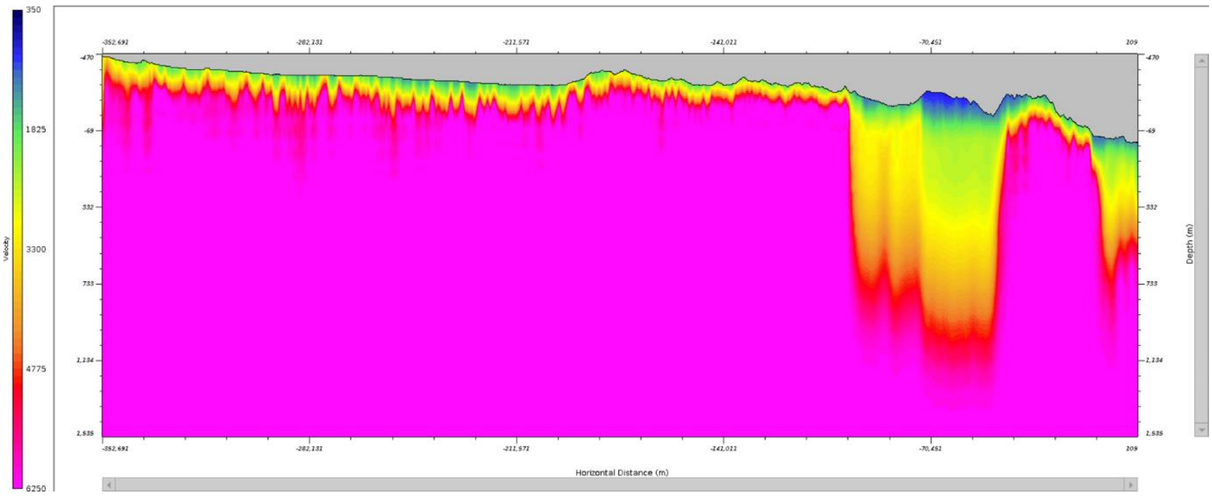


Figure 9. MW1 Refraction tomography velocity model. East (left), West (right).

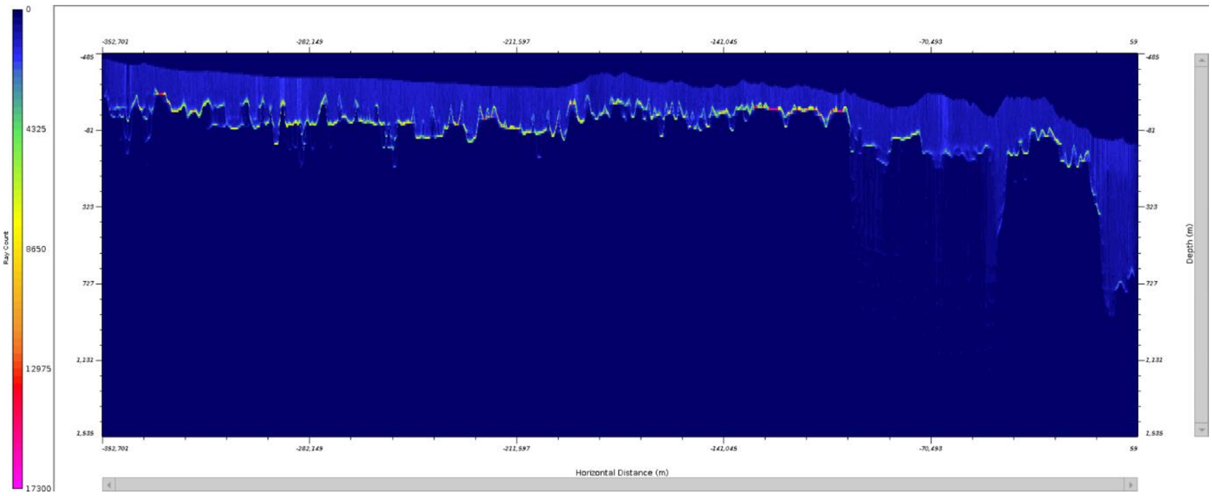


Figure 10. MW1 Refraction tomography ray tracing model. East (left), West (right).

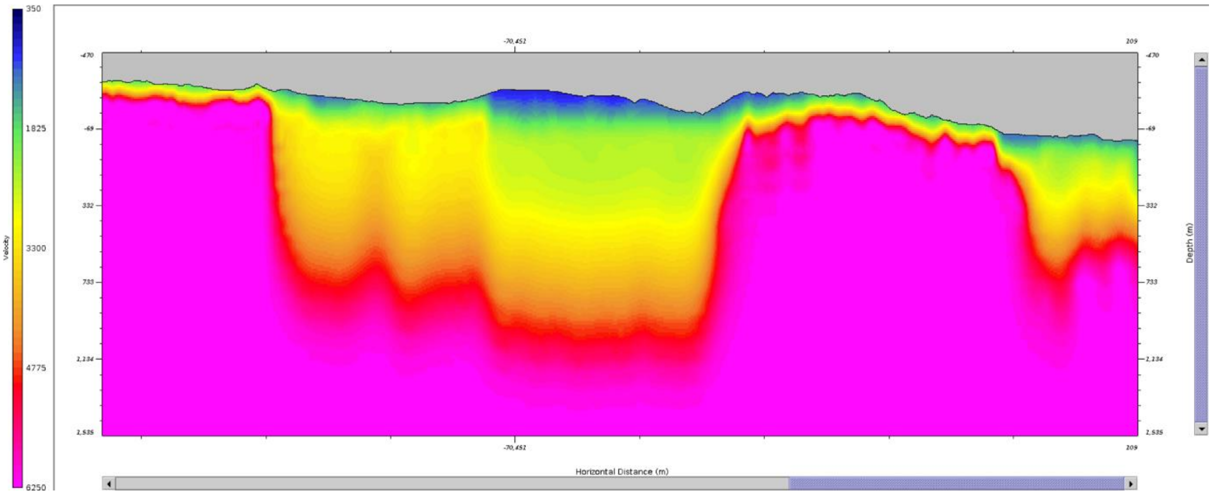


Figure 11. MW1 Refraction tomography velocity, zoomed to Perth Basin. East (left), West (right).

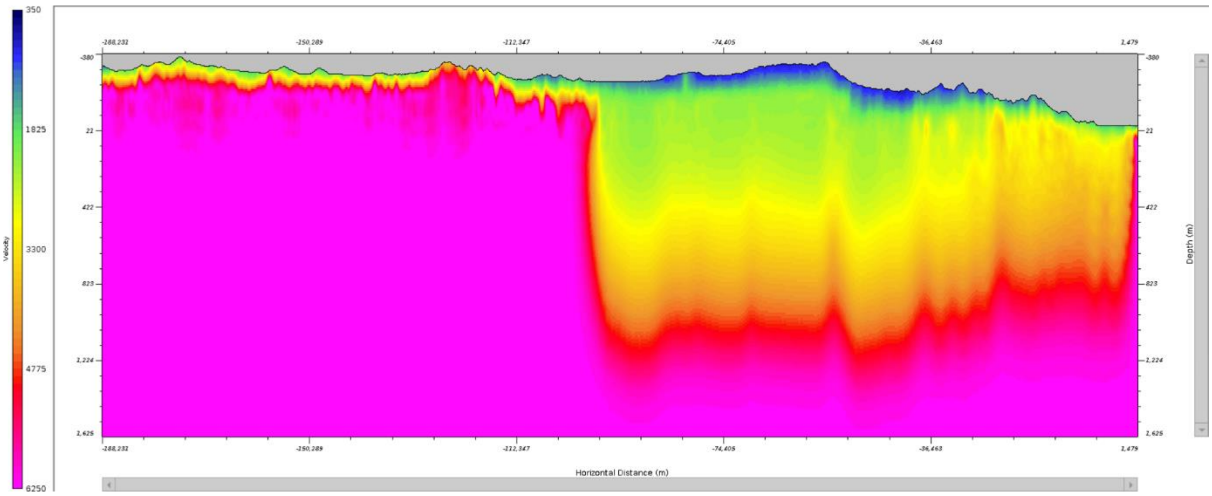


Figure 12. MW2 Refraction tomography velocity model. East (left), West (right).

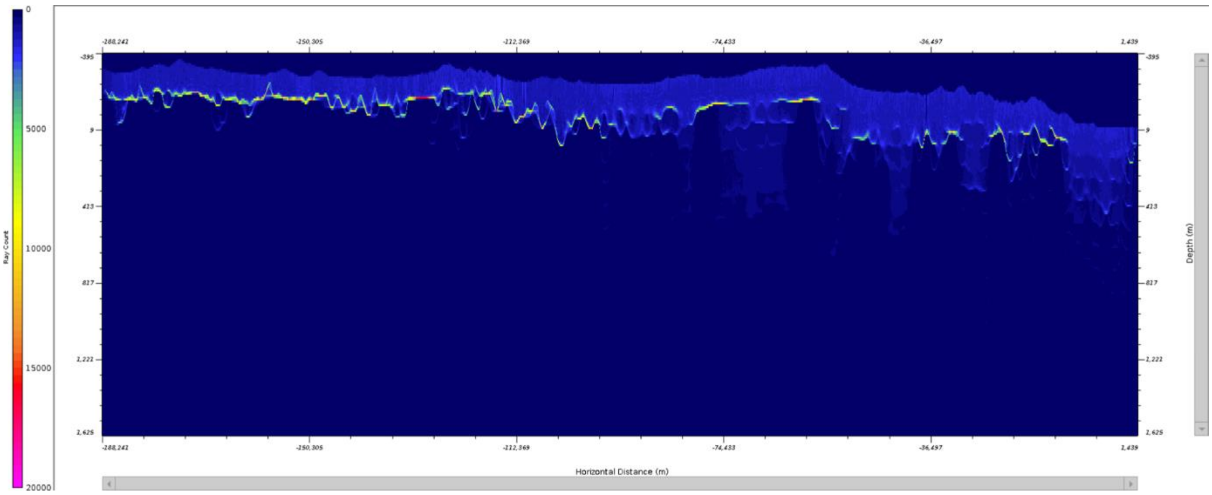


Figure 13. MW2 Refraction tomography ray tracing model. East (left), West (right).

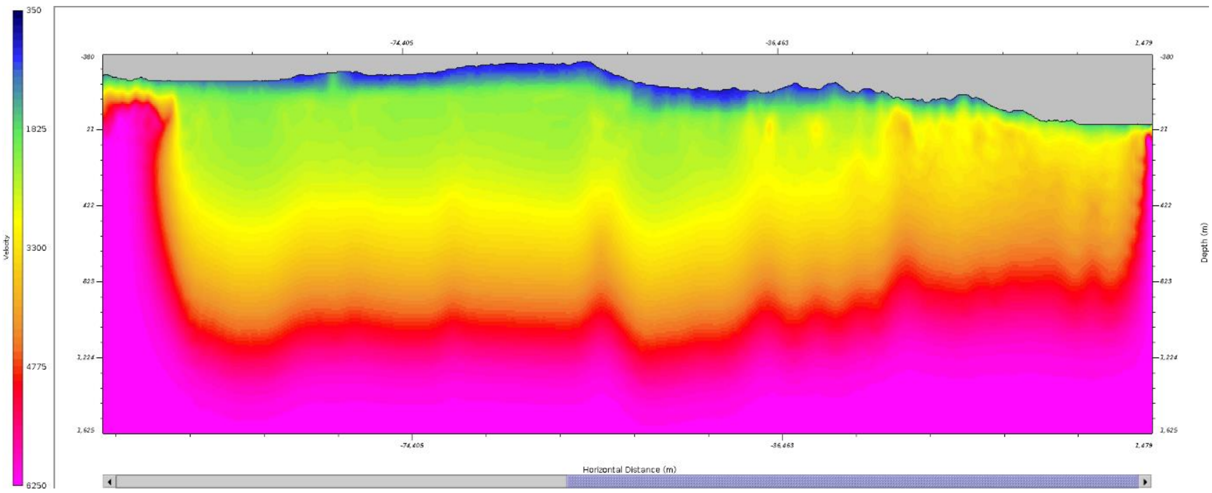


Figure 14. MW2 Refraction tomography velocity, zoomed to Perth Basin. East (left), West (right).

## 3.5 PRE-PROCESSING

At the completion of the first break picking and refraction tomography, data was imported to the processing software. The pre-processing workflow included several processes designed to remove noise, enhance signal, and prepare the data for migration. Where required the data was wrapped in a temporarily applied gain of T^1.1 and offset^1.1.

### 3.5.1 Vehicle noise attenuation

Vehicles were a strong source of noise throughout the survey. Given the length of the active spread and shot intervals between sweeps it was not feasible to halt traffic during recording. During a sweep, vehicles travelling along the spread pass several receivers. On the subsequent sweep those vehicles are moving past a different set of receivers. By sorting the data into common receiver domain, small groups of noise affected traces are positioned next to clean data. Using this sorting, a time-frequency denoise (TFDN) process can be used to attenuate the noise on the affected traces. Figure 15 below shows an example of receiver gathers before vehicle noise attenuation. Figure 16 show the noise attenuation applied in common receiver domain.

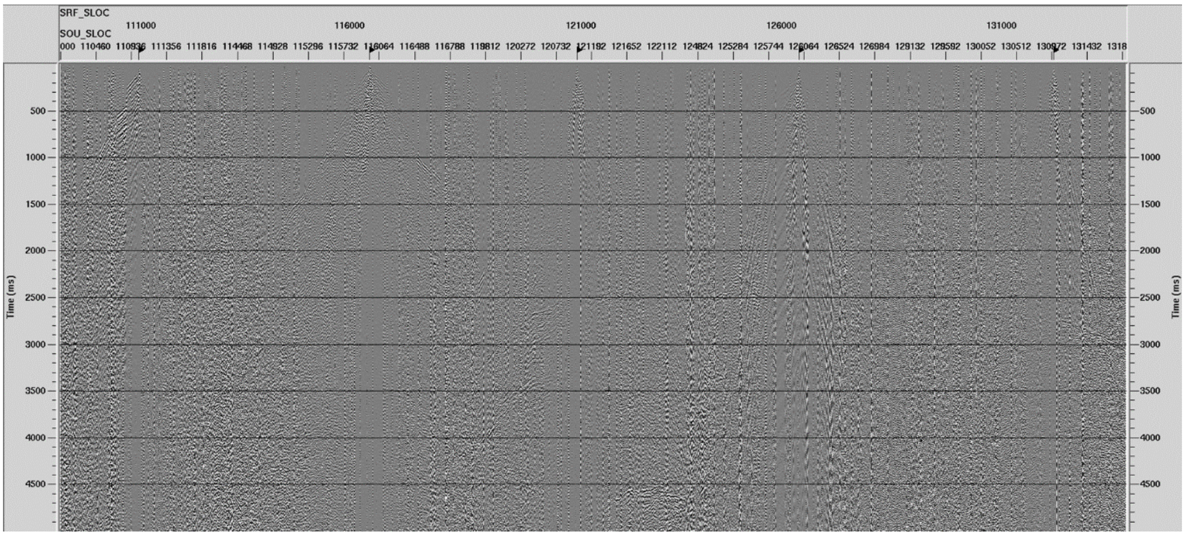


Figure 15. Input to vehicle noise attenuation.

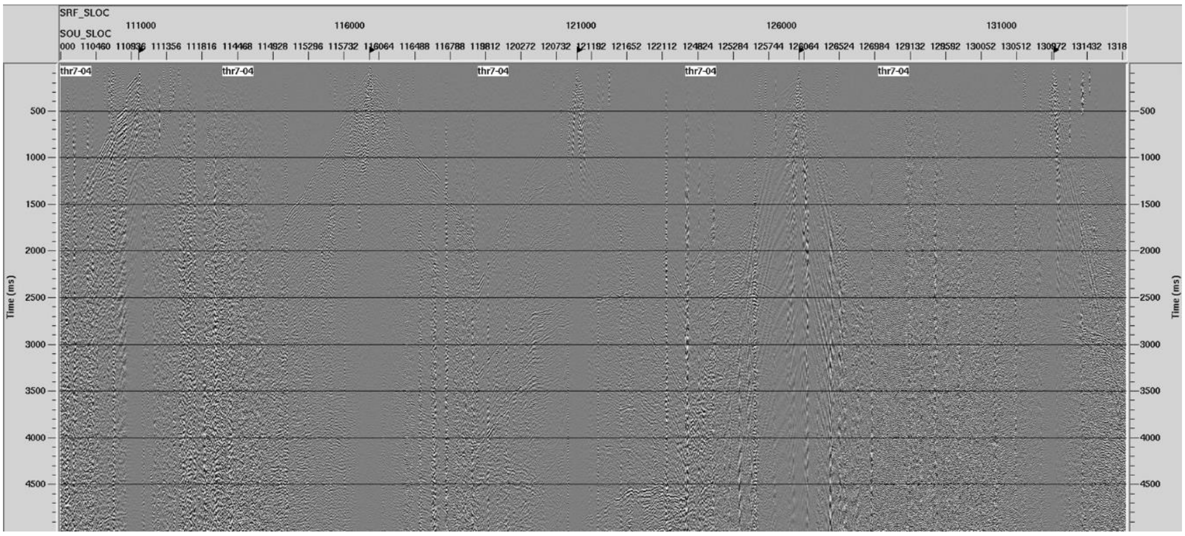


Figure 16. Vehicle noise attenuation applied.

### 3.5.2 Refraction Statics

Statics are corrections applied to seismic data to compensate for the effects of variations in elevation, near-surface low-velocity-layer (weathering) thickness, weathering velocity, and/or to shift data to a reference datum. In this workflow the refraction statics to floating datum were applied prior to air blast attenuation and zero-phase spike deconvolution and surface wave noise attenuation. This allows for better noise attenuation as surface waves become more linear once statics are applied.

Application of statics used results calculated from the mean CDP delay time method. First break picks with an offset range greater than 150m were used in the calculation. A 5800m/s replacement velocity was used for both lines. A final datum elevation of 460m was used for MW1 and 370m for MW2 to calculate static shifts to the floating datum for processing. Figure 17 and Figure 18 (MW1), and Figure 19 and Figure 20 (MW2) show the source and receiver static to final datum respectively.

The chosen replacement velocity of 5800m/s is not ideal for the Perth Basin as the refractor in the basin is in fact much slower (around 2100m/s). However, the vast majority of the line is over a hard rock environment which requires the faster replacement velocity. Imaging in the basin does appears slightly degraded from the use of this replacement velocity. However, depth migration, as explained in section 4, was performed from topography removing the assumption of replacement velocity and final datum.

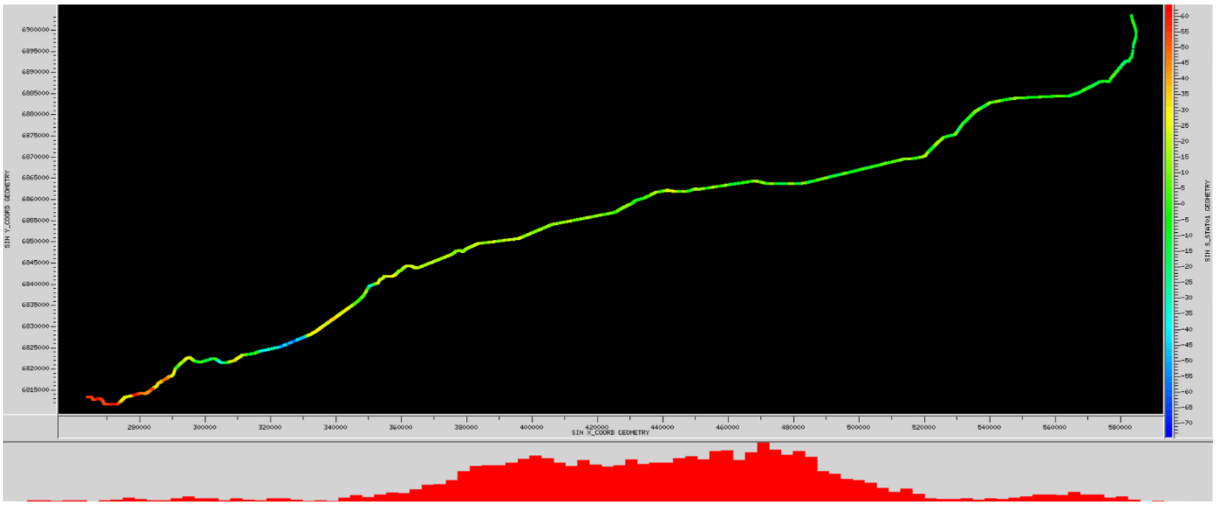

Figure 17. MW1 source refraction static to final datum.

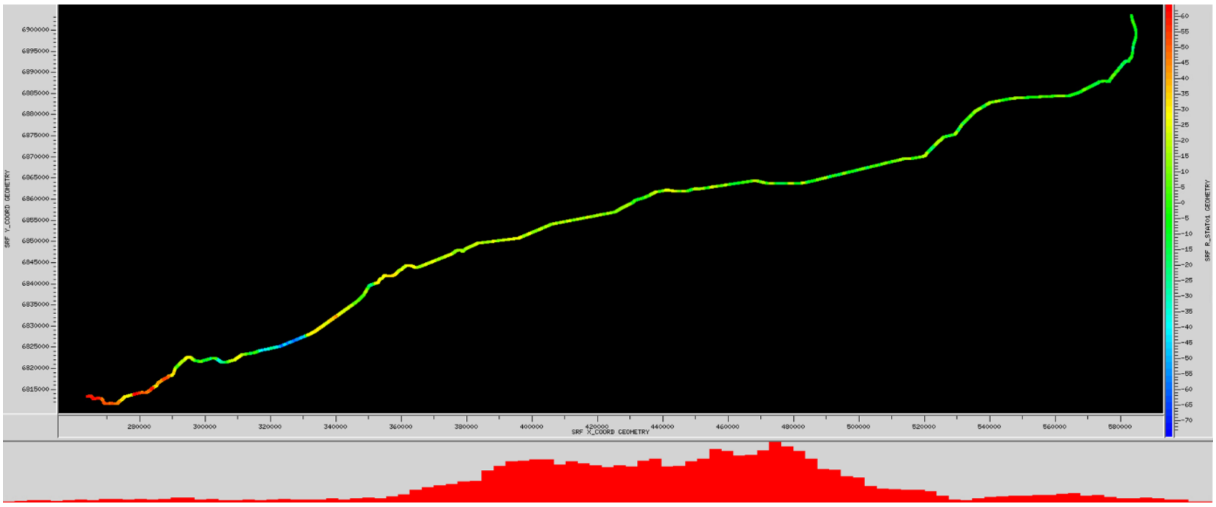

Figure 18. MW1 receiver refraction static to final datum

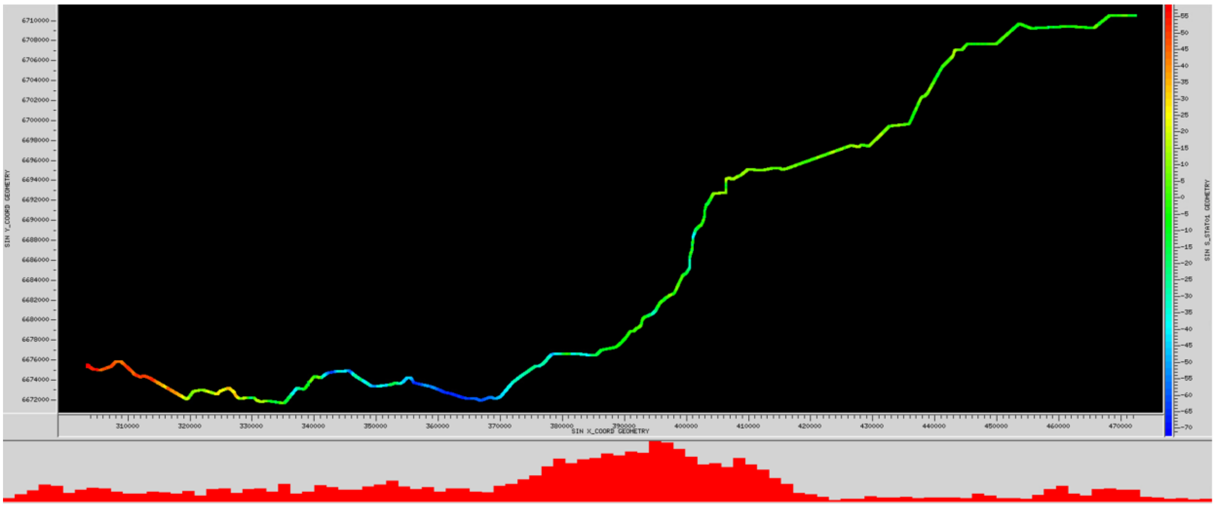

Figure 19: MW2 source refraction static to final datum

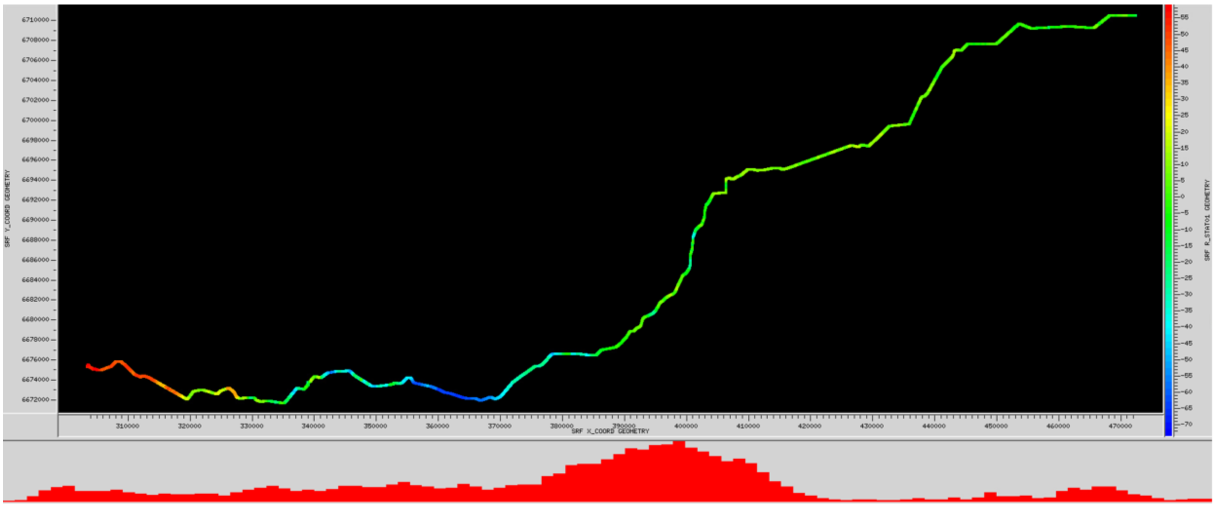

Figure 20: MW2 receiver refraction static to final datum

### 3.5.3 Deconvolution

The recorded seismic signal may be considered as a convolution of the source signal with the instruments, geophones, and earth response. This signal often includes undesirable effects such as reverberation, attenuation, and ghosting that mask the primary reflection (Robinson et al, 2008). Deconvolution aims to remove these effects, whitening the spectrum and increasing temporal resolution.

A zero-phase spike deconvolution using a 100ms operator length was applied to the data as seen in Figure 21 and Figure 22. The resulting data is zero-phase with a flatter, more broadband frequency-amplitude spectrum. The whitening of the frequency-amplitude spectrum, Figure 22 inset, gives the appearance of attenuating the high amplitude, low frequency noise associated with ground roll.

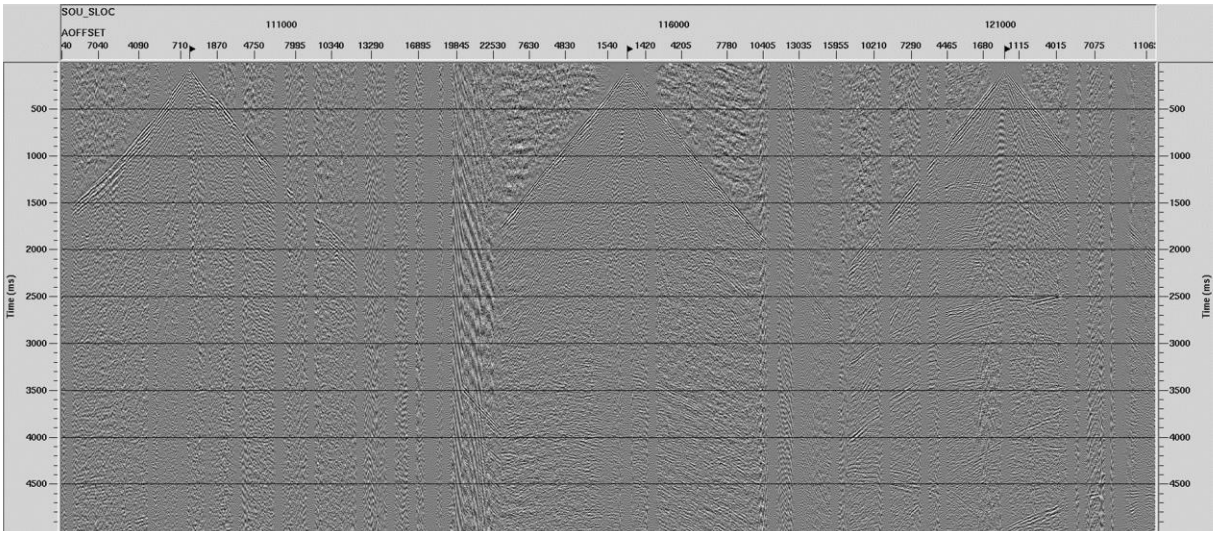


Figure 21. Data prior to zero-phase spike deconvolution

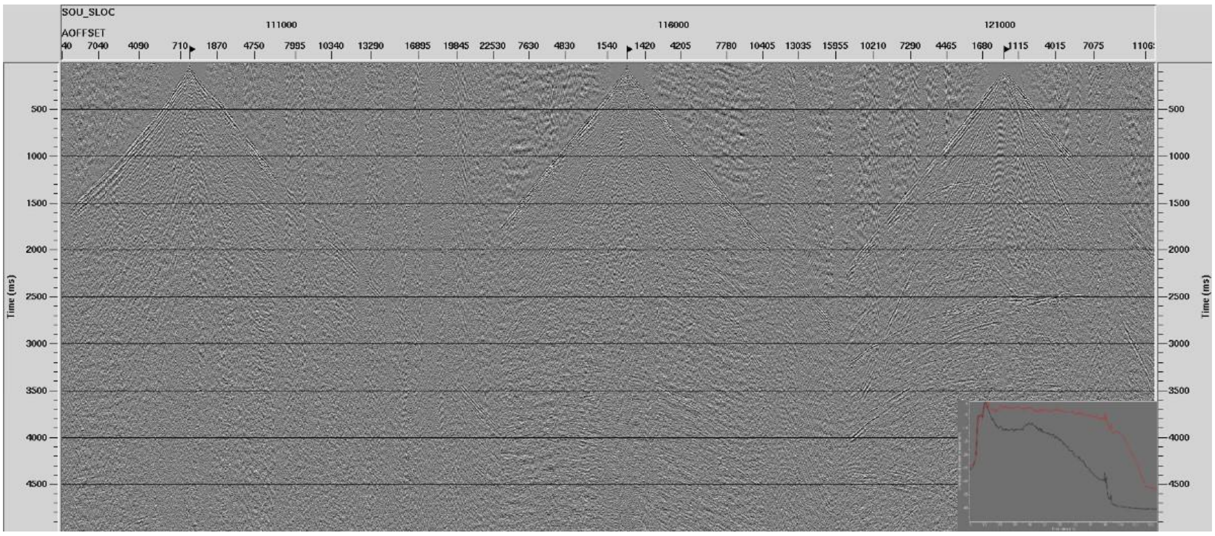


Figure 22. Zero-phase spike deconvolution applied.

### 3.5.4 Airblast Attenuation

Air blast attenuation was applied using a velocity of 345m/s for MW1. For MW2, velocities of 345m/s, 350m/s, and 355m/s were used to ensure more complete attenuation of the noise. The process operates trace by trace, searching for anomalous amplitudes over a window centred on the theoretical two-way-time calculated from the defined velocity. The effect of air blast attenuation can be observed in the images of cumulative noise attenuation shown in Figure 23 and Figure 24.

### 3.5.5 Surface wave noise attenuation

The strongest noise type in land seismic is typically the ground roll energy. It is comprised of surface waves or modified Rayleigh waves which are characterised by broad bandwidth, high amplitude, and a low velocity (after Sheriff et al, 1995).

Surface wave noise attenuation (SWNA) was performed in shot domain wrapped within an 100ms AGC. Two seismic domains were identified, the craton and the basin, which contained surface waves propagating at different velocities. In the craton area a target velocity of 2800m/s was used, and in the basin areas 1200 m/s was used for MW1, and 1000 m/s was used for MW2. The effect of SWNA can be observed in the images of cumulative noise attenuation shown in Figure 23 and Figure 24.

### 3.5.6 Despike TFDN

Spikes remaining in the data after the above processes may be attenuated using a secondary pass of time-frequency denoise (TFDN) in the shot domain. TFDN despike was performed in shot domain between 0 and 1500ms using a 5-trace window, over frequencies from 0 Hz to 125 Hz and temporal widow of 500ms.

Data was then passed through a statistical analysis where an RMS amplitude was calculated over 2 windows. The absolute amplitude and RMS ratio between windows were used compared against a threshold value and traces outside of that threshold were killed. The effect of TFDN can be observed in the images of cumulative noise attenuation shown in Figure 23 and Figure 24.

The MW2 line presented with some residual spikes, which were not entirely removed in the vehicle noise attenuation process. To address this an additional pass of despike TFDN was applied in receiver domain for MW2 only.

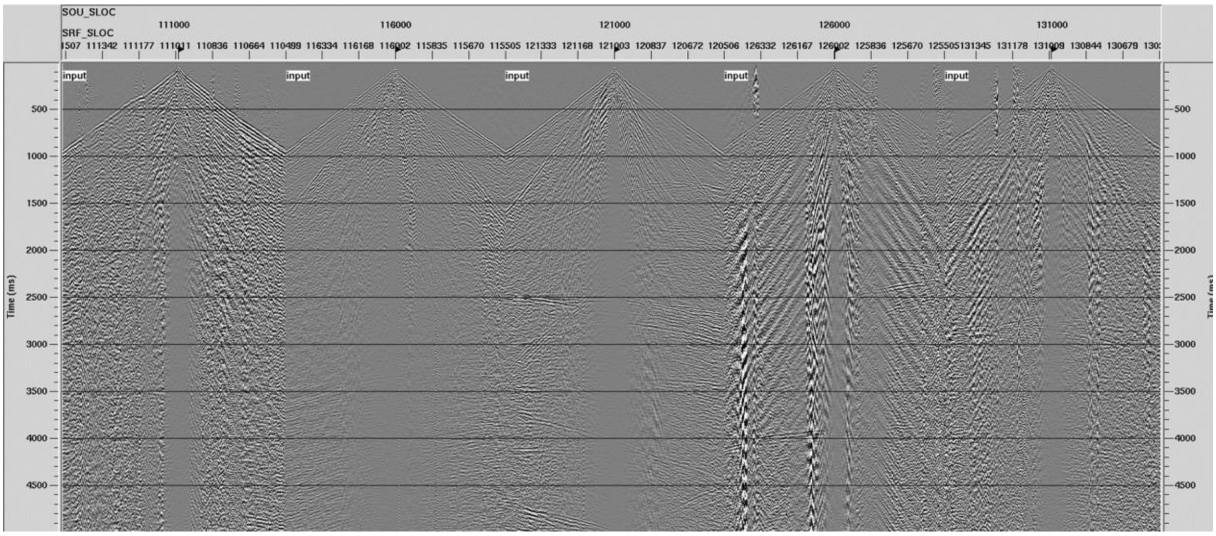


Figure 23. Input to noise attenuation.

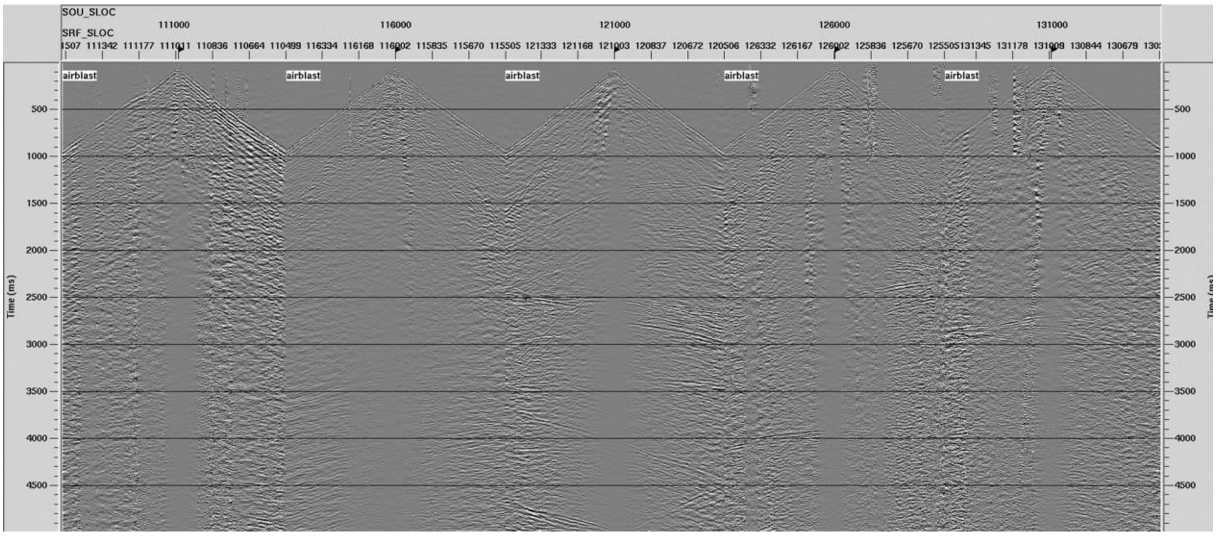


Figure 24. Decon, Air blast, SWNA, TFDN applied.

### 3.5.7 Dip Filter

For the MW2 data, remaining linear noise was identified in the basin areas. This was further attenuated after the above processes using dip filtering. Dip filtering applies a spatial filter in the f-x domain using specified frequencies and velocities. The filtering was tapered on to protect the near surface data.

Filtering was applied in the shot domain, wrapped within a 100ms AGC. Two velocity filters of 1000-1200-3400-3600m/s and 200-300-900-1000m/s within a 2-4-90-100Hz frequency filter were applied.

### 3.5.8 Residual statics

Noise attenuated shots were sorted to CDP gathers and NMO corrected using the initial velocity model. Data were conditioned with an AGC, linear noise attenuation and bandpass filter. Residual statics were then calculated using an 11 CDP smash was used to generate pilot traces. The calculation window used was a flat 4 second window centred on 3 seconds.

### 3.5.9 Amplitude scaling

Variations in amplitude can be caused by differences in source or receiver coupling, noise, or differences in near surface conditions which affect attenuation. Two observations were made relating to amplitude scaling along the MW1 and MW2 lines. Firstly, there was significant vehicle noise which varied in intensity along the line. Secondly the line transitions from hard rock in the east to sedimentary basin in the west which exhibits higher than expected levels of attenuation.

Following noise attenuation, Surface Consistent Amplitude Compensation (SCAC) was tested using source, receiver and offset terms. The SCAC test was migrated and compared with data which used a

4000ms AGC and removal of $T^{1.1}$ prior to migration. SCAC provided inconsistent results along the line, whereas the AGC method appeared more robust. The long window used in this method partially preserves the amplitudes while accounting for noise and absorption. After careful consideration processing proceeded using the AGC method.

## 3.6 VELOCITY ANALYSIS

A critical step in seismic processing is Interactive Velocity Analysis (IVA). The velocity defined through IVA is used to NMO correct the gathers for stacking, residual statics calculation and in the final migration. For this project, after defining the initial velocity model using constant velocity stacks, 3 iterations of IVA were performed.

### 3.6.1 Initial velocity model

The initial velocity model was derived from constant velocity stacks (CVS), where a suite of stacks are produced using a single velocity function. From the reflectivity apparent in these stacks a time and spatially varying velocity can be coarsely defined forming the initial velocity model. This initial velocity model was used in the production of noise attenuation QC stacks and residual statics as described in 3.5.8 Residual statics.

### 3.6.2 1st pass IVA

Noise attenuated shots were sorted to CDP gathers and NMO corrected using the initial velocity model. Gathers were conditioned before producing super-gathers at a 5km interval. Interactive velocity analysis was used to define a velocity model down to 8 seconds.

Figure 25 shows the first pass IVA from the hard-rock craton area. As expected, the velocity trend is much faster than that of the Perth Basin shown in Figure 26.

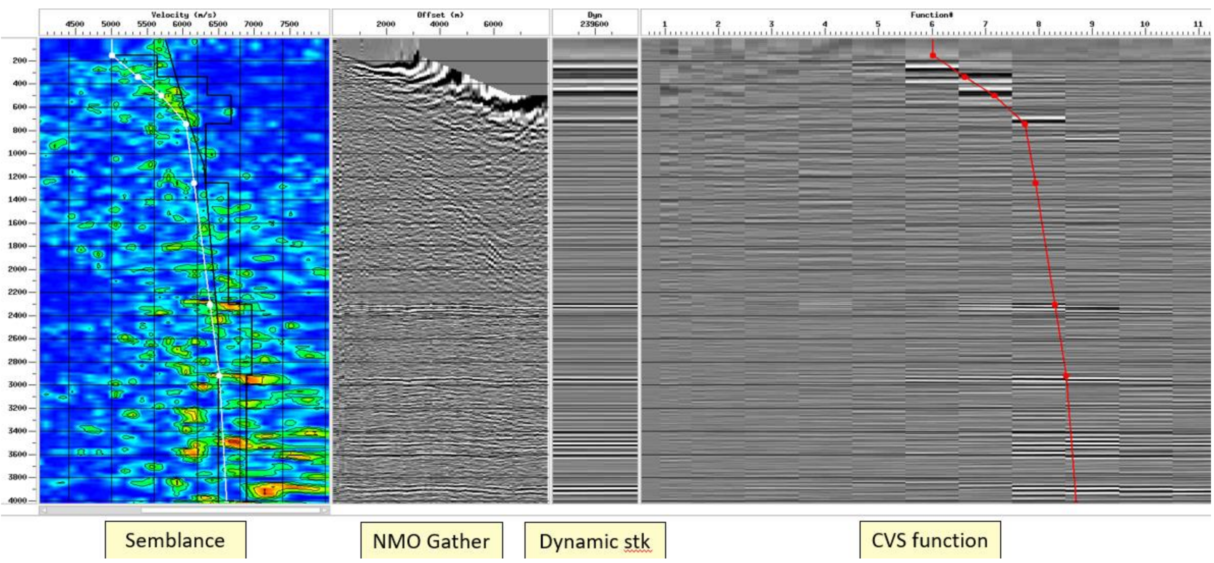


Figure 25. Interactive Velocity Analysis (IVA) from craton area (MW1).

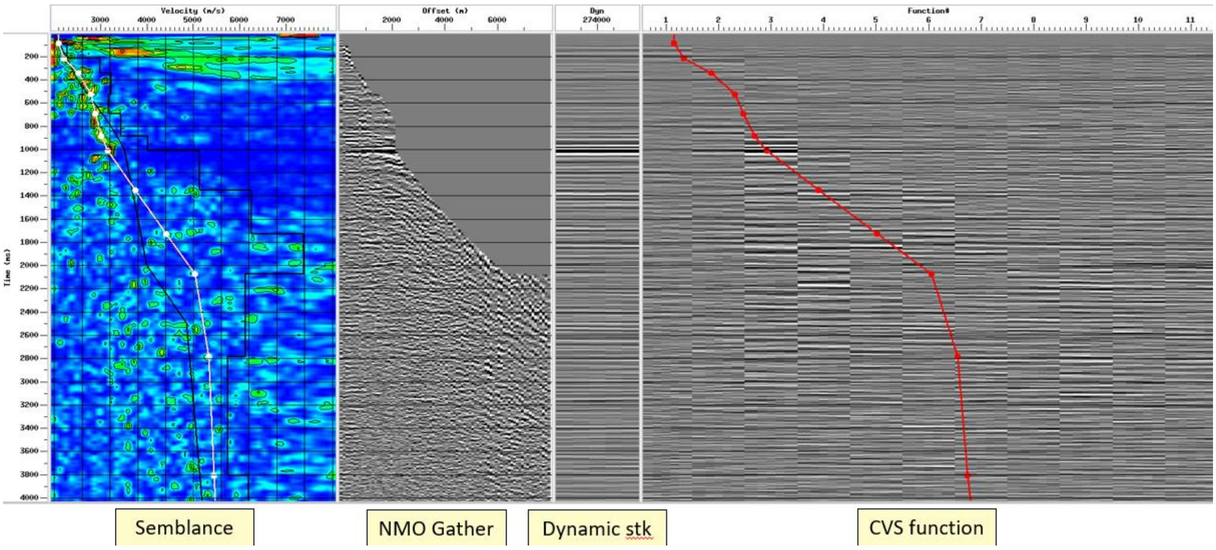


Figure 26. Interactive Velocity Analysis (IVA) from Perth Basin (MW1).

### 3.6.3 2nd pass IVA

The noise attenuated data had 2nd pass residual statics applied and was shifted to final datum before migration of every 5th CDP using the 1st pass IVA velocity. The second pass of IVA was then performed using the migrated gathers, picking at an interval of 2km.

### 3.6.4 3rd pass IVA

The noise attenuated data had 2nd pass residual statics applied and was shifted to final data before migration of every 5th CDP using the 2nd pass IVA velocity. The third pass of IVA was then performed using the migrated gathers, with a focus on picking the Perth Basin at an interval of 1km.

These 3rd pass velocities, shown in Figure 27 (MW1) and Figure 28 (MW2), were used in the final Pre-stack Time Migration. A heavily smoothed version of these velocities was also used in the time-depth conversion as explained in section 3.9.

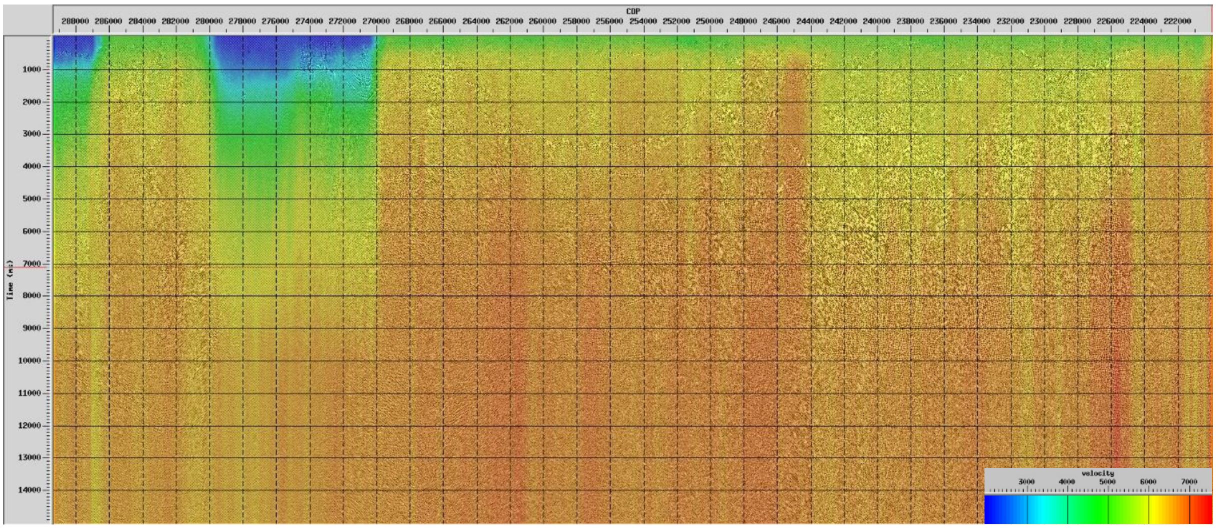


Figure 27. MW1 Final PreSTM RMS velocity overlain on the migrated stack.

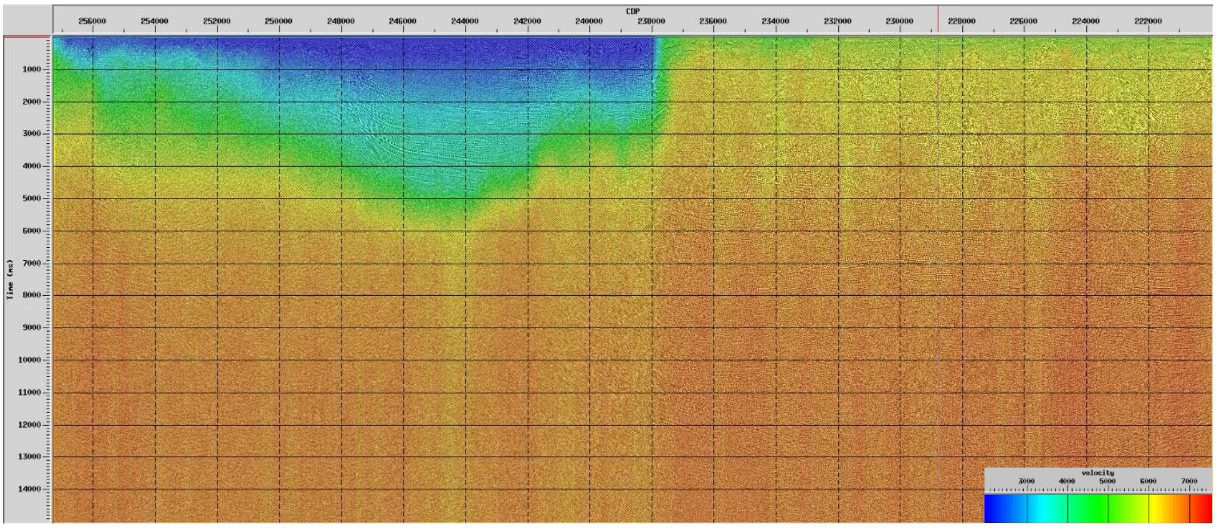


Figure 28: MW2 Final PreSTM RMS velocity overlain on the migrated stack

## 3.7 KIRCHHOFF PRESTM

The Kirchhoff Pre-stack Time Migration (K-PreSTM) algorithm is suited to imaging moderately complex geologies with a gradually varying velocity field. K-PreSTM produces seismic images in terms of travel-time rather than depth and must then be converted using a velocity model to approximate depth. Prior to final migration, a suite of tests was performed to determine the optimal migration aperture and dip limit.

K-PreSTM was performed from final datum (460m) for MW1, and floating datum for MW2, using an output CMP spacing of 5m and offset binning of 50m-10050m x 25m. A 15km half-aperture was used with a 75deg dip limit. This larger than typical migration aperture takes advantage of the long offsets beyond the minimum 8km offset with the aim of imaging deeper events.

# 3.8 POST MIGRATION PROCESSING

## 3.8.1 Gather conditioning

Linear noise attenuation was applied to migrated gathers, targeting steeply dipping events with a velocity of 5000m/s.

A post-migration amplitude balance was performed tailored to each of the 8 second and 20second record length datasets. For the 8 second dataset a 500ms AGC was used, which helps to enhance the shallow features of the dataset. On the 20 second dataset a 3000ms AGC was applied, balancing the amplitudes but without damaging contrast of deeper events such as the Moho.

## 3.8.2 High-density velocity analysis (HDVA)

Following noise attenuation a high-density velocity analysis HDVA was undertaken. Gathers were reviewed at 500m intervals, and where necessary the velocity model was adjusted to correct any excessive moveout. The migration velocity was removed from the gathers and the HDVA velocity was applied.

## 3.8.3 Trace muting

Inner and outer mutes applied to the migrated gathers change the contribution of different offsets to the stacked image. For gathers limited to 8 seconds, angle mutes as, explained in Table 5, were used to produce near, mid, far, and full stacks.

When applying angle mutes the record length is typically truncated as a result. Hence angle mutes were not applied when producing the stack with a 20 second record length. For this product, only a 2-degree inner mute was applied along with the hand-picked outer mute.

Table 5. Mute parameters

| 8 second data mute parameters | |
|---|---|
| Near | 0 – 15 degrees |
| Mid | 15 – 30 degrees |
| Far | 30 – 45 degrees |
| Full | 0 – hand-picked outer |

## 3.8.4 Stacking

Stacking was performed using a $1/n^x$ normalisation where n is the number of samples being summed. The number of samples can be raised to a power, in this case the exponent used is 0.5. MW2 was shifted to final datum post stack at this point in processing.

The stack output at this point is referred to as the raw stack.

### 3.8.5 Post-stack conditioning

Post-stack conditioning included random noise attenuation, time-varying bandpass filtering, coherence filtering and time-varying gain. To attenuate random noise an F-X deconvolution process was applied. This used a 31-trace window, 10% white noise and a 750ms temporal window.

As the signal is returned from the earth higher frequencies are attenuated more rapidly with depth. As a result, a time-varying bandpass filter can be employed to remove noise at frequencies above what is expected for signals at depth. The filter was applied using the parameters in Table 6 below. The filters are linearly interpolated between the defined points.

Table 6. Time-varying bandpass filter

| CDP | Filter | Application time |
|---|---|---|
| 220000 | 10-20-80-100 | 0 – 300 ms |
| | 4-8-80-100 | 400 – 20000 ms |
| 271000 | 10-20-80-100 | 0 – 300 ms |
| | 4-8-80-100 | 400 – 20000 ms |
| 273000 | 2-4-80-100 | 0 – 300 ms |
| | 2-4-80-100 | 400 – 20000 ms |
| 281000 | 10-20-80-100 | 0 – 300 ms |
| | 4-8-80-100 | 400 – 20000 ms |
| 289254 | 10-20-80-100 | 0 – 300 ms |
| | 4-8-80-100 | 400 – 20000 ms |

A coherence filter was used to enhance the signal by estimating the continuity of events over a spatial window. For the 8 second record length data a 21-trace window was used with a dip limit of 7ms/trace. For the 20 second record length data a 21-trace window was used with a dip limit of 9ms/trace with the aim to improve continuity of deeper events.

With the goals of improving the strength of near surface events and more evenly balancing amplitudes, a time-varying gain was applied to the 8 second stack using -8dB/s from 0 to 1000ms.

A record length (single scalar) AGC was applied to the 20 second stacks. This laterally balances the amplitudes of the stack along the line.

## 3.9 TIME-DEPTH CONVERSION

The final PreSTM velocity model was smoothed using a 5km smoother. The purpose of smoothing the velocity is to reduce sharp lateral velocity changes that can result in anomalous pull-up and push downs in the depth converted section. Because of the discrepancy between the replacement velocity, 5800m/s and the actual refractor velocity, ~3000m/s, it was necessary to clip the minimum velocity for depth conversion. Several tests were performed to assess the clip value resulting in the selection of a minimum velocity of 3000m/s. This provided an acceptable mistie in depth. However, problems such as this replacement velocity discrepancy and sharp lateral velocity change as seen at the Darling Scarp are best addressed using Pre-Stack depth Migration.

## 3.10 FINAL PRESTM STACKS

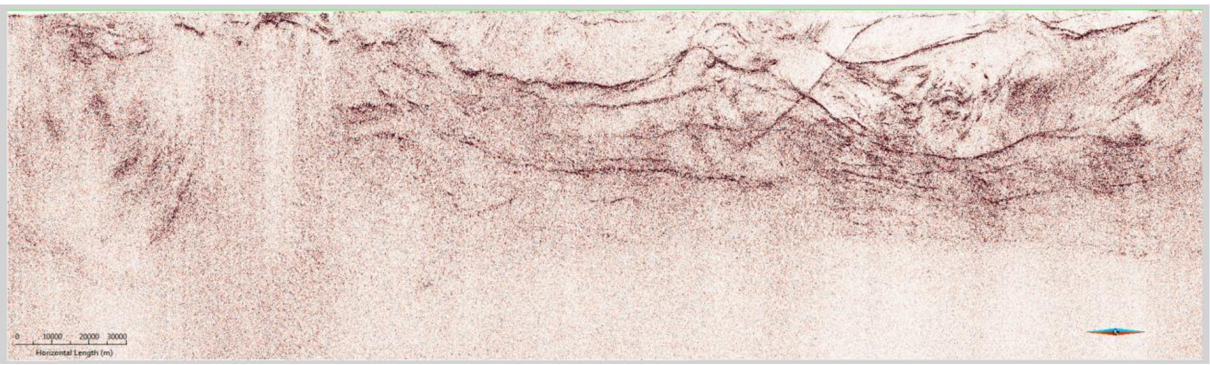

Figure 29. MW1 PreSTM Full stack, 20 seconds

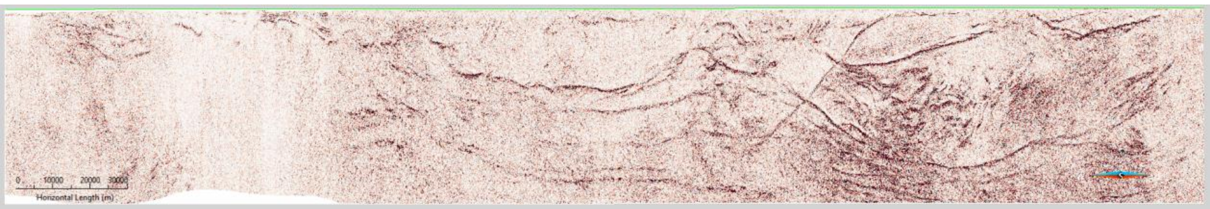

Figure 30. MW1 PreSTM Full stack, 8 seconds

Figure 31. MW1 PreSTM Near stack, 8 seconds

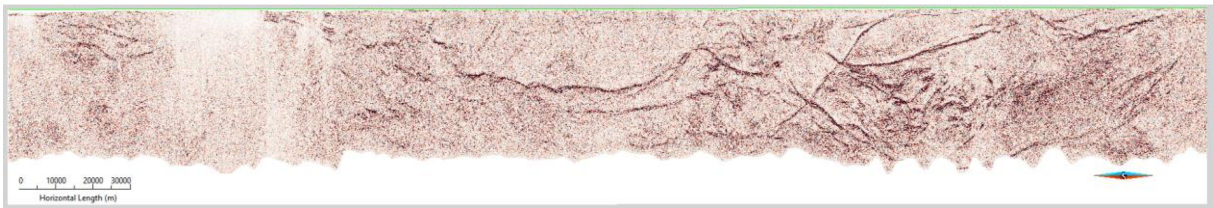

Figure 32. MW1 PreSTM Mid stack, 8 seconds

Figure 33. MW1 PreSTM Far stack, 8 seconds

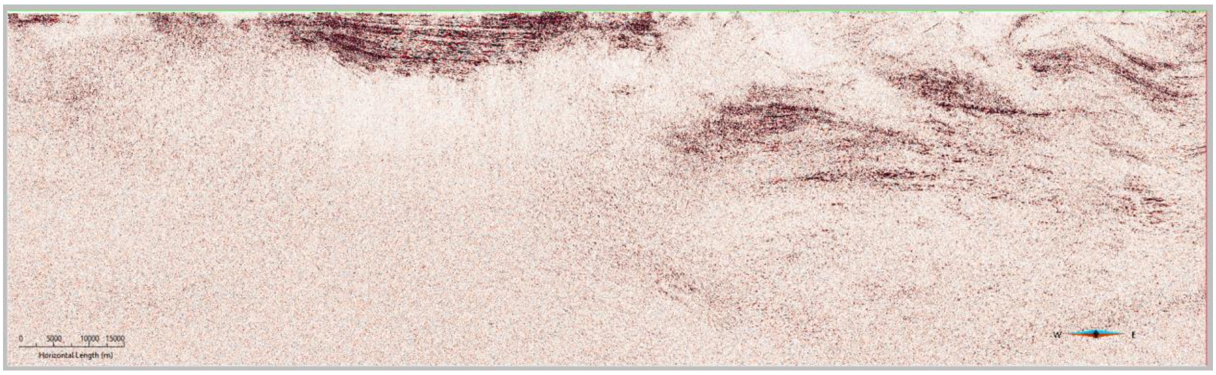


Figure 34. MW2 PreSTM Full stack, 20 seconds

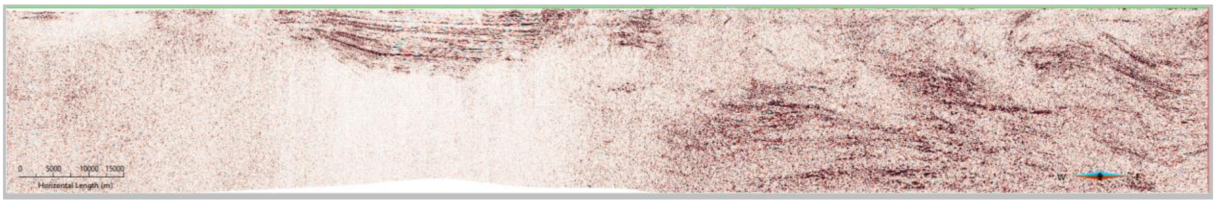


Figure 35. MW2 PreSTM Full stack, 8 seconds


Figure 36. MW2 PreSTM Near stack, 8 seconds

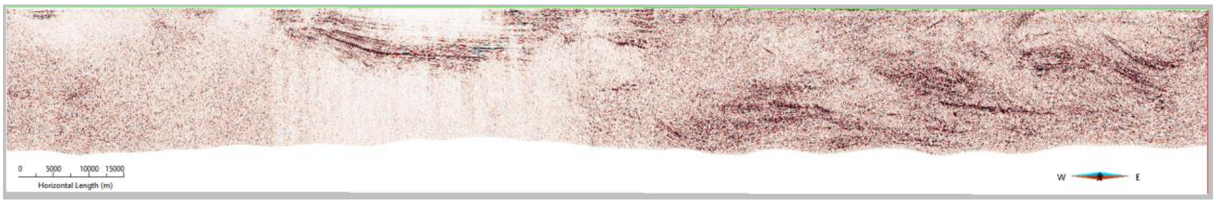


Figure 37. MW2 PreSTM Mid stack, 8 seconds

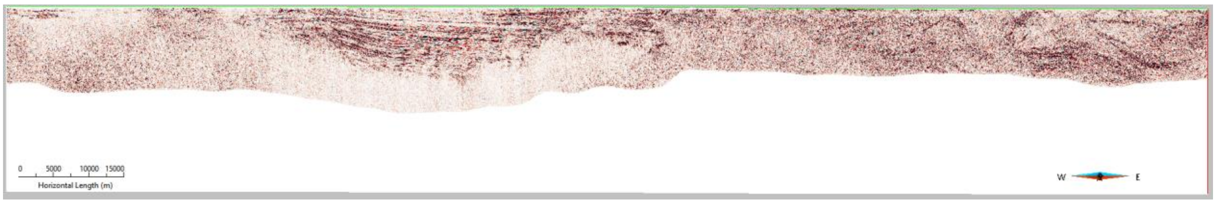


Figure 38. MW2 PreSTM Far stack, 8 seconds

# 4 DEPTH IMAGING

The imaging algorithm known as Kirchhoff Pre-stack Depth Migration (K-PreSDM) has the potential to address non-hyperbolic moveout resulting from lateral velocity variations, providing accurate depth positioning for seismic images. A depth imaging method proposed by Ziramov et al. (2022) was used, which is uniquely suited to a hard rock environment and utilises both refraction and reflection tomography for velocity model building (VMB).

The depth imaging workflow is illustrated in Figure 39 below.

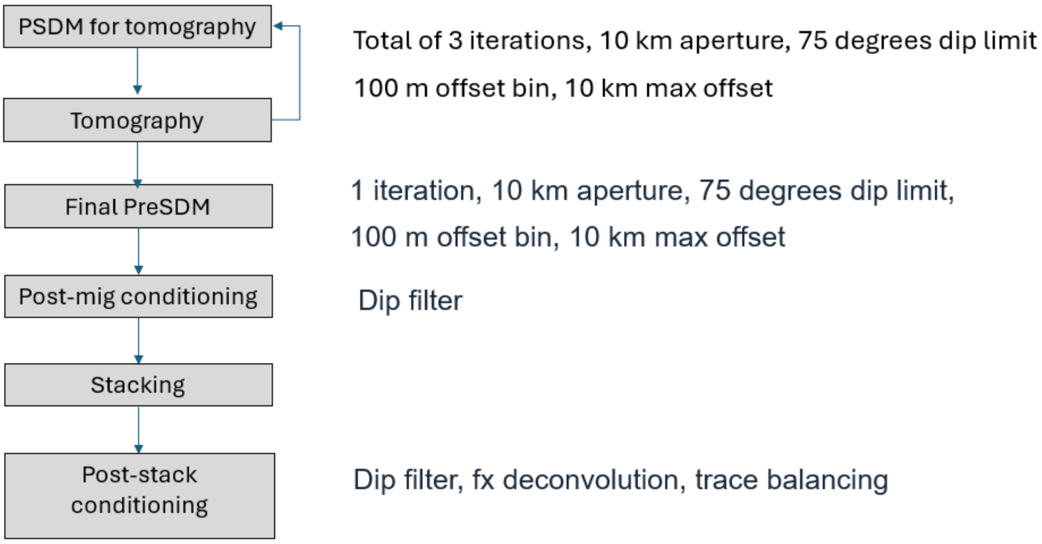


Figure 39. Depth imaging workflow.

Table 7. K-PreSDM processing flow.

| K-PreSDM Processing Flow | |
|---|---|
| 1. | Pre-processed data input, with AGC and removed gain $T^{1.1}$ |
| 2. | Pre-Stack Depth Migration for velocity updates, 3 iterations |
| 3. | RMO picking and reflection tomography 3 iterations |
| 4. | Final K-PreSDM: 5m CDP bin spacing,<br>10km half-aperture, 75deg dip |
| 5. | Post-migration spatially varying top mute and AGC 10km window |
| 6. | CDP Stack |
| 7. | Post-stack filtering.<br>Depth variant bandpass filter<br>Dip filter (Tau-Pi based +-9 dip, 21 traces aperture), F-X deconvolution (9 trace aperture 2 applications), AGC 50km window (single scalar trace balance) |

## 4.1 INITIAL VELOCITY MODEL

The velocities obtained from time imaging are transformed to interval in depth using the Dix equation. A shallow velocity model derived from refraction tomography is scaled and merged with the transformed time imaging velocity. The maximum interval velocity was clipped to 7000 m/s and the entire field was smoothed using a 1.5 km lateral and 400 m vertical smoother. This formed the initial velocity that was further refined thought several iterations of depth imaging and reflection tomography, Figure 40 and Figure 41 below.

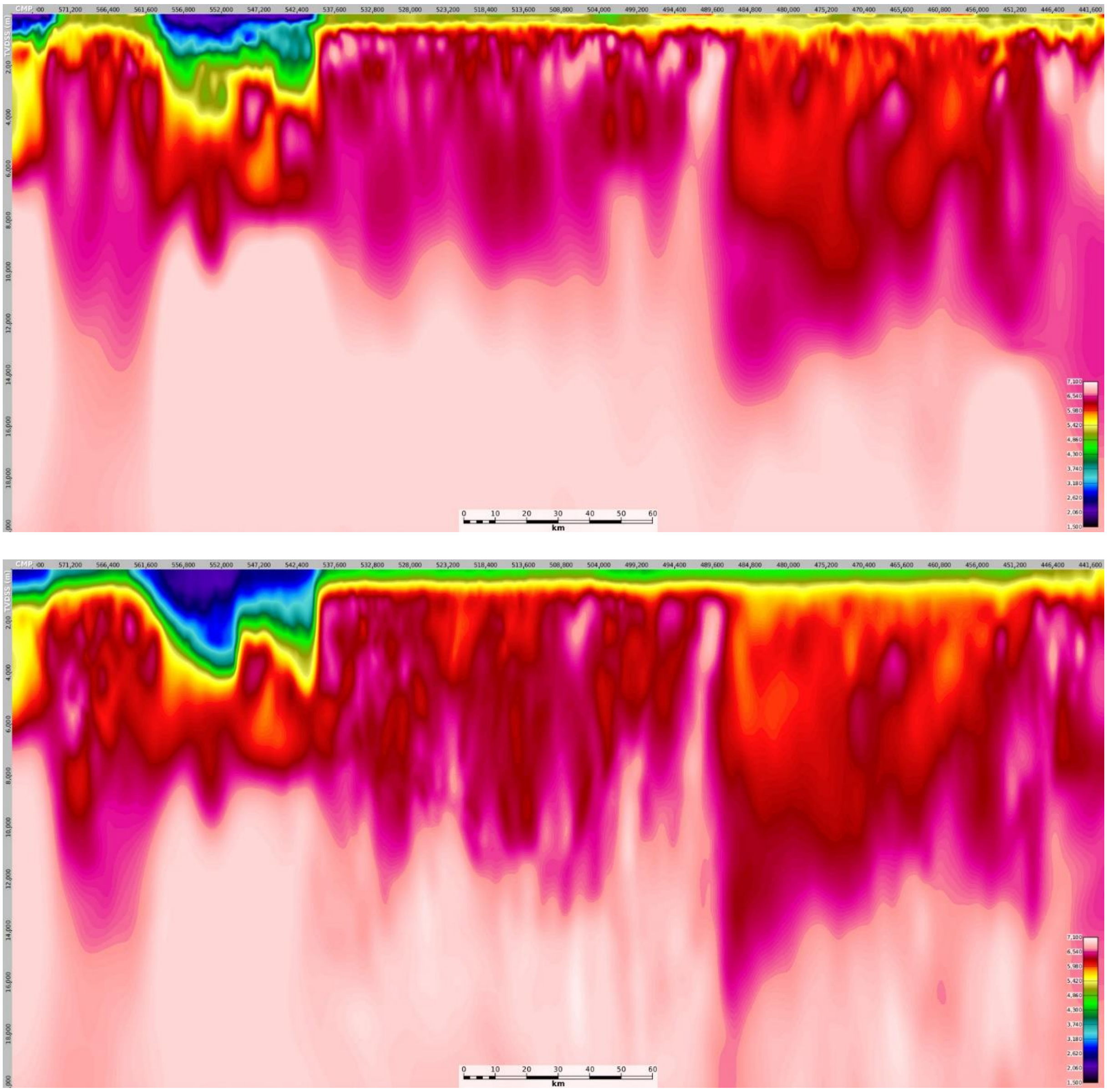


Figure 40. MW1 starting velocity model (top), MW1 final velocity model for depth imaging (bottom).

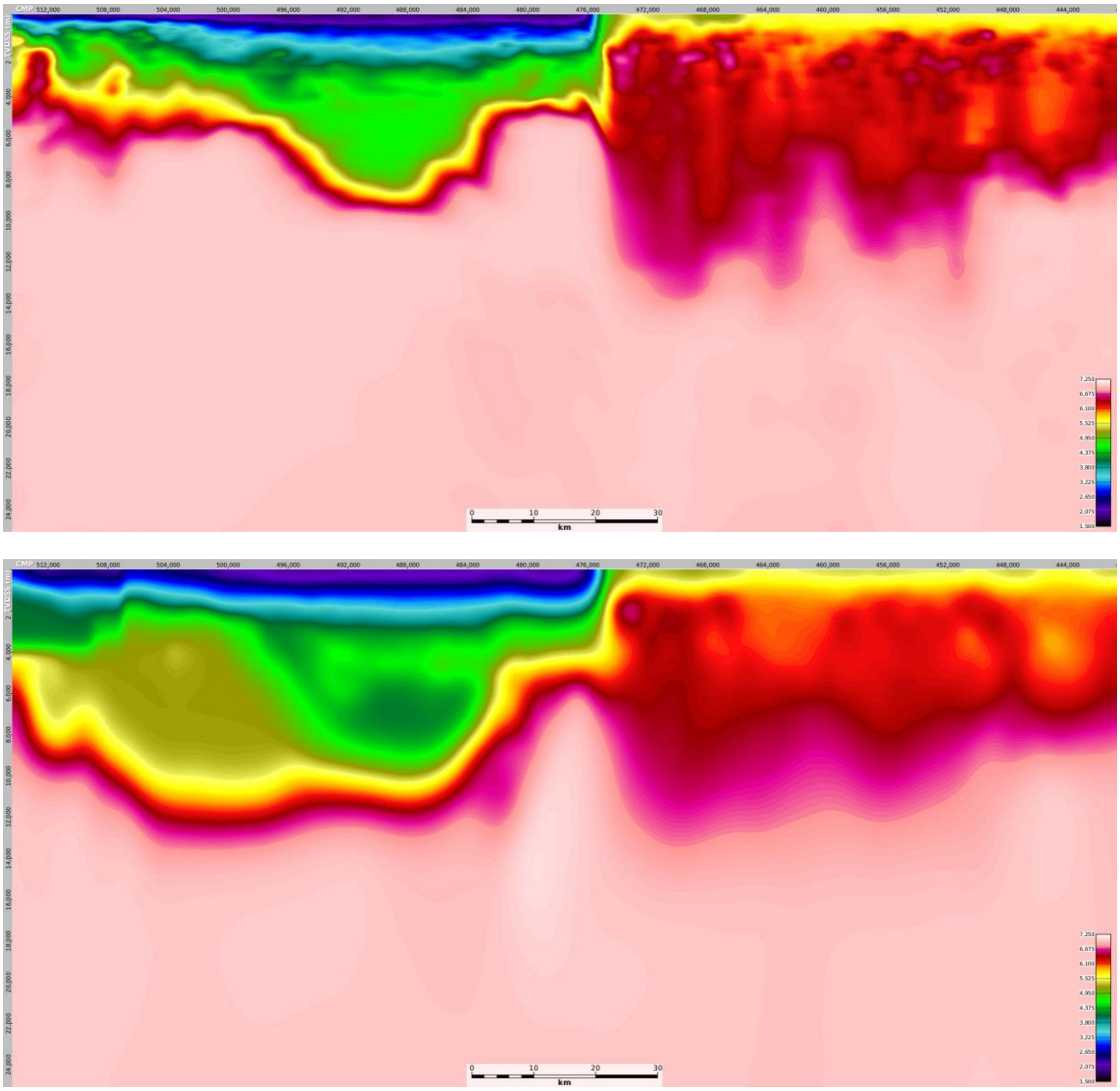

Figure 41. MW2 starting velocity model (top), MW2 final velocity model for depth imaging (bottom).

## 4.2 TOMOGRAPHIC VELOCITY UPDATES

The technique of pre-stack reflection tomography involves multiple iterations of residual moveout (RMO) analysis applied to depth-migrated Common-Image-Point (CIP) gathers for updating an initial model. Automatic estimation of hyperbolic RMO is derived from CIP gathers, following the methodology detailed by Woodward et al. (2008). Initial iterations primarily focused on rectifying velocity discrepancies in shallow zones before progressing downwards to update the entire velocity model. Each subsequent iteration calculated an updated velocity model, minimizing the observed residual moveout, as described by Tanis et al. (2006). The final velocity model following 3 iterations of tomography is shown below for MW1 in Figure 42 and Figure 43. For MW2 the final velocity model is overlain on the final stack in Figure 44

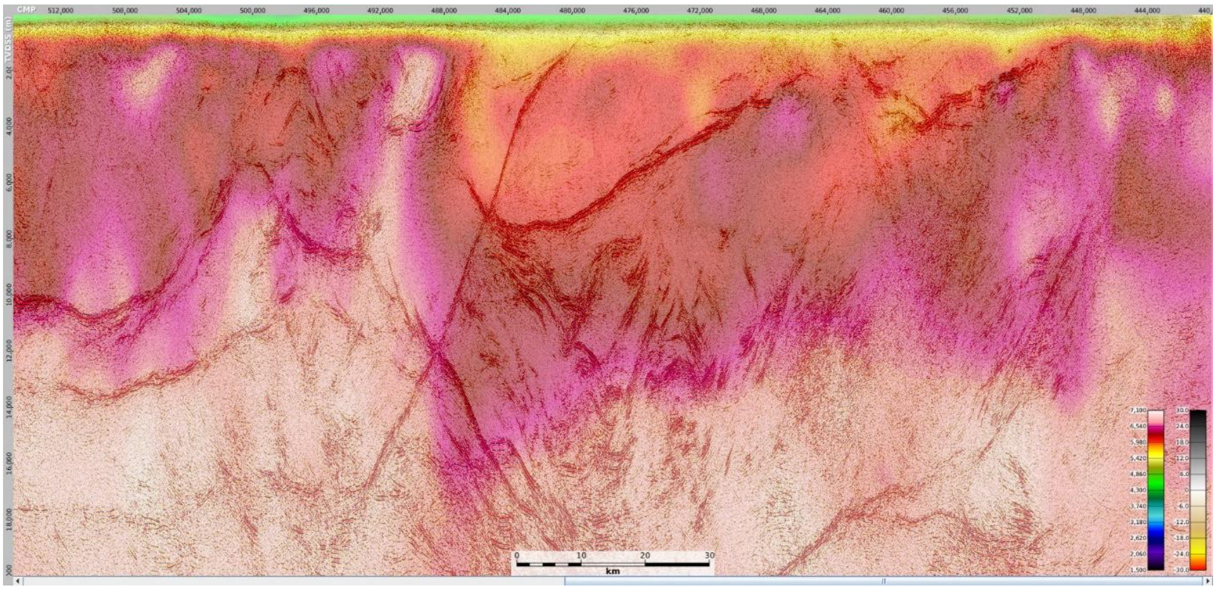

Figure 42. Eastern end of MW1 PSDM Stack overlain with final velocity model.

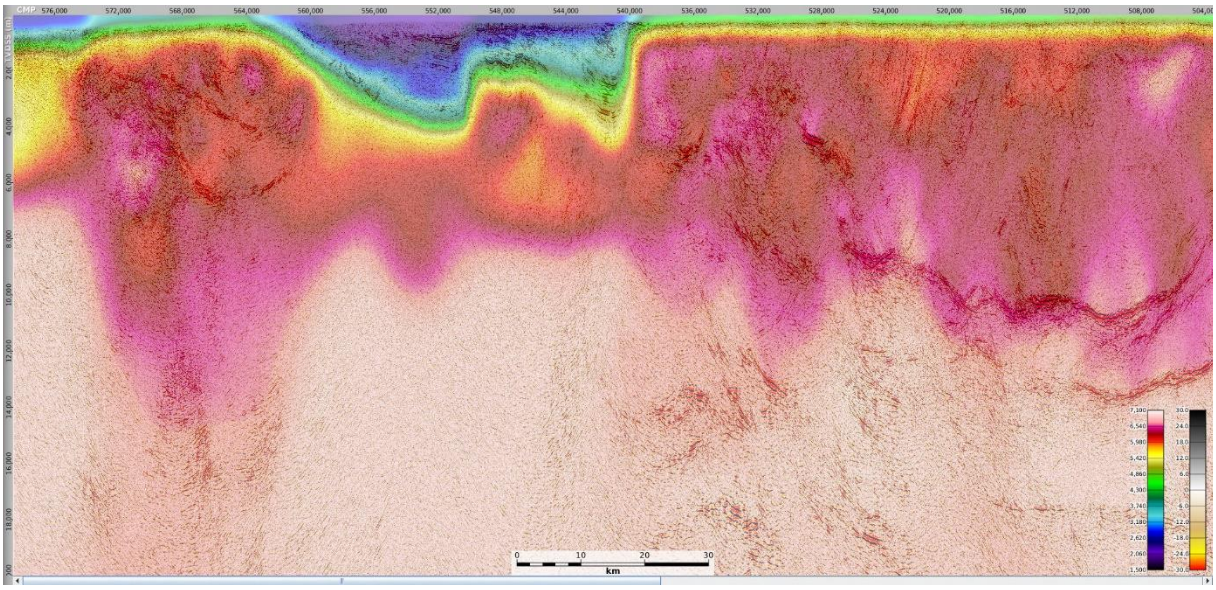

Figure 43. Western end of MW1 PSDM Stack overlain with final velocity model.

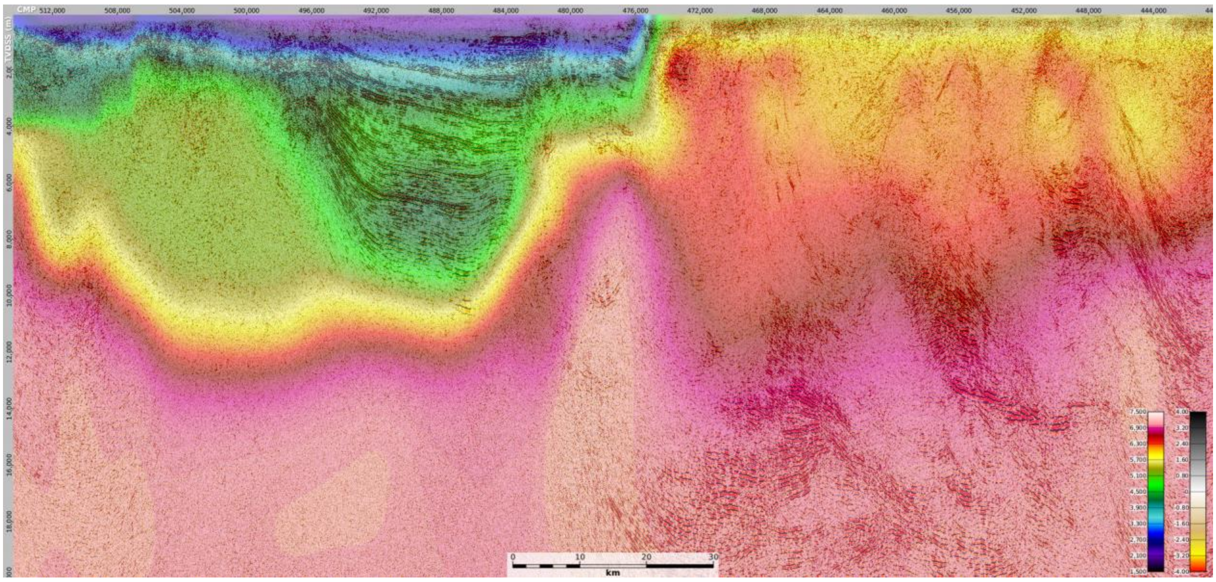

Figure 44. MW2 PSDM Stack overlain with final velocity model

To ensure accuracy, this model is compared to nearby FWS logs sourced from reliable measurements in existing drillholes. While the Mungarra-1 well shown in Figure 45 is some distance offline, it penetrates the same formations as observed on MW1, and shows a close match between the logged and seismic velocity. For MW2 no well logs were made available, however, QC against geological cross sections and a seabase “depth to basement” horizon aided in validation of the model.

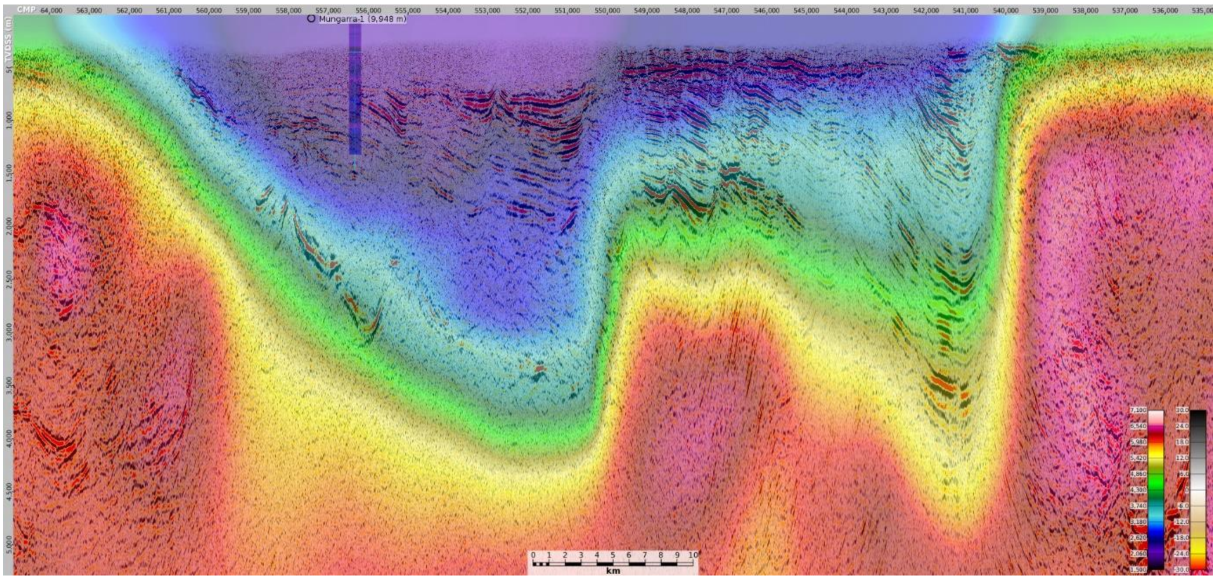


Figure 45. Close up into PSDM Stack overlain with final velocity model and provided sonic logs.

## 4.3 KIRCHHOFF PRESDM

The K-PreSDM algorithm relies on ray tracing, and the seismic image is generated through diffraction summation. It demonstrates versatility by effectively handling data across a wide frequency range, particularly beneficial in scenarios where high resolution is paramount. Notably, it has fewer dip limitations and is better able to handle rapid, lateral velocity changes.

Successful implementation requires substantial S-R offsets, robust reflectivity, and Common-Image-Point (CIP) gathers that have undergone migration with a suitable initial velocity model. The accuracy of this initial velocity model, particularly in the near surface, is crucial, as a deficiency in trace fold and small S-R offsets can impede the reflection tomography's ability to update the velocity model.

Unlike with time imaging techniques, depth imaging does not require assumption of replacement velocity to migrate data from surface to final datum. As migration is in depth domain, we use measured source/receiver elevations to image data to a final flat datum of 460m (MW1) and 370m (MW2). Together with accurate velocity model and superior imaging algorithm, depth imaging provided high-precision mapping in both the hard rock and Perth Basin areas.

## 4.4 POST MIGRATION PROCESSING

K-PreSDM data passed through additional post-migration processes (see above in Table 7) to remove unwanted noise and artefacts on the migrated gathers and improve reflectivity of the stack. The flow included depth varying gain and bandpass filtering, random noise attenuation and coherency filtering.

## 4.5 FINAL PRESDM STACKS

The Figures below show full PreSDM stacks for MW1 (Figure 46) and MW2 (Figure 47).

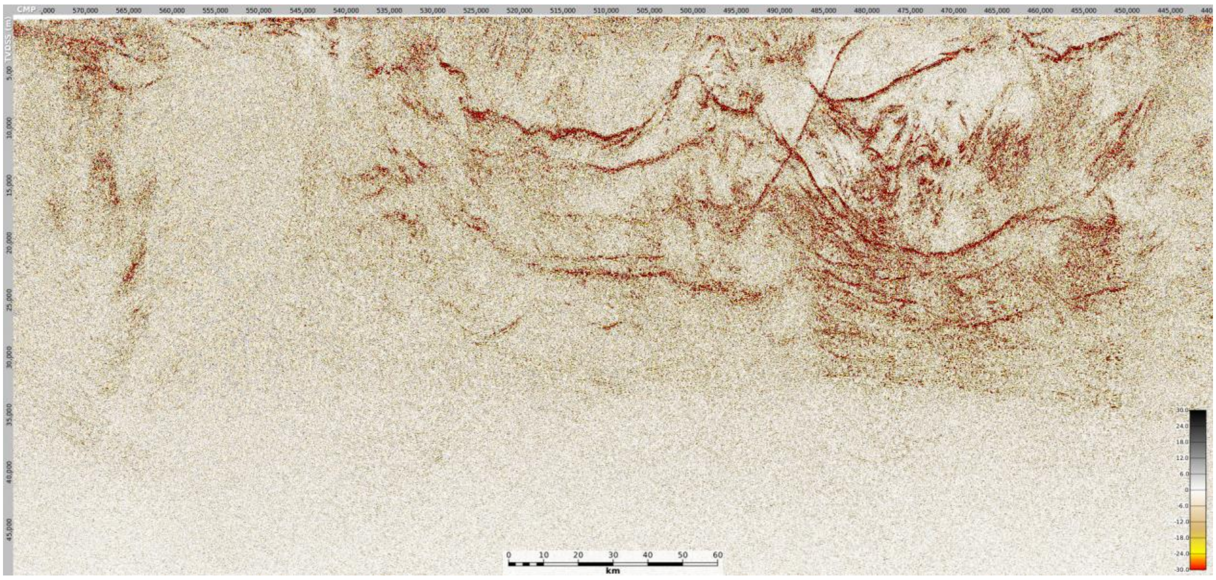

Figure 46. Raw PreSDM stack

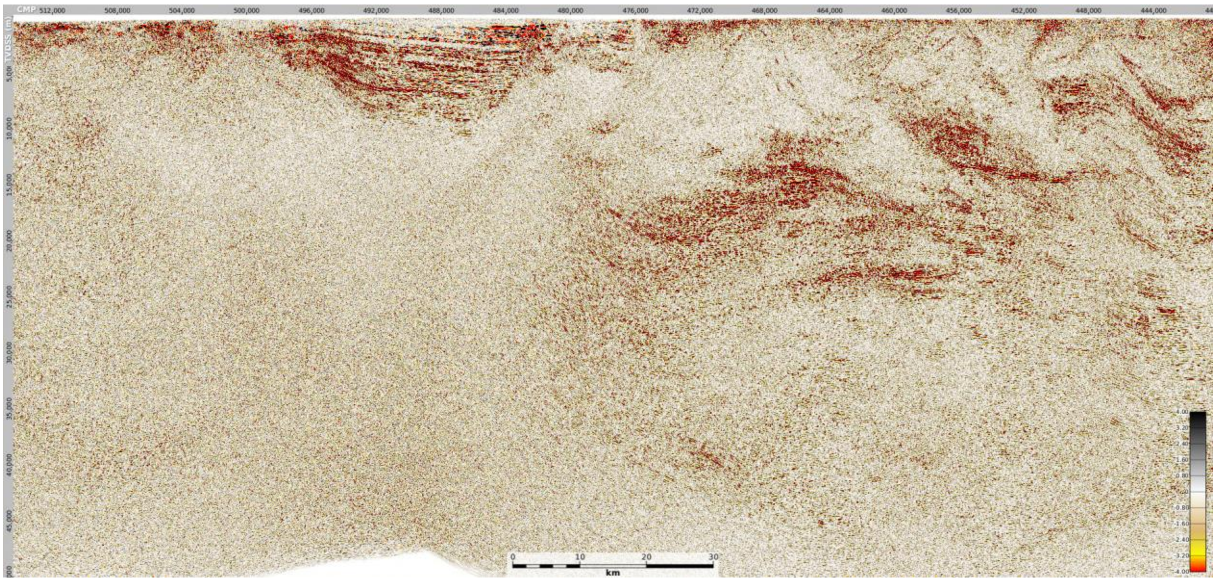

Figure 47. Final PreSDM stack

# 5 CONCLUSIONS

Overall, the data quality along the 23GSWA-MW1 and 23GSWA-MW2 lines is considered high. While vehicle noise is spread along the length of the survey, each of the instances affected an isolated number of channels. Noise was reduced through Geraldton by shooting during the night while there was less traffic. After noise attenuation these affected channels do not appear to impact the image. The all-active acquisition which provided additional long offsets out to approximately 30km appears to have benefited both the deep image and steeply dipping shallow events.

Seismic processing through the comprehensive pre-processing and PreSTM workflow generated two final subsurface images which focused on shallow and deep targets, respectively. The shallow image is complimented by three angle stacks, providing additional insight. The time migrated images were also supplied in depth after being converted using a smoothed version of the migration velocity.

Data was also passed through a Depth Imaging workflow which included 3 iterations of RMO picking and reflection tomography to update the velocity model. The final Kirchhoff Pre-stack Depth Migration and post-migration processing yielded significant uplift at line bends and areas of sharp lateral velocity contrast, particularly near the Darling Scarp and through the Perth Basin. In some locations the basin sands appear to have high levels of attenuation. The long offsets acquired appear to have aided the PreSDM workflow in imaging the basin areas.

These images revealed notable features along the entire seismic line, including the geometry of the Perth Basin, the continuity and character of major faults, such as the Darling Fault, and the crustal architecture of the Yilgarn Craton. Highly complex structures are visible on MW1 between Mt Magnet and Yalgoo. The Moho is clearly defined to the east but becomes less clearly imaged as the line proceeds west over the Perth Basin.

Some recommendations are made for future seismic surveys.

1. Resampling for Improved Efficiency: The MW-1 and MW2 seismic lines represent large datasets due to their length, high trace density, long record length, and a fine 2ms sample rate. While the 2ms sample rate was maintained throughout processing, the maximum sweep frequency used was only 96Hz. In such cases, resampling the data to 4ms can significantly improve processing runtimes and reduce disk space requirements by half. This resampling would not degrade the seismic bandwidth or resolution as the highest recoverable frequency content is well below the Nyquist frequency defined by the original 2ms sample rate. Implementing this approach in future surveys with similar acquisition parameters would enhance processing efficiency without compromising data quality.

2. Targeted Infill Shooting: The infill shots acquired on either side of exclusion zones where standard seismic acquisition was not permitted appear to have limited impact on image quality within those gaps. These additional shots could have been more strategically deployed within the Perth Basin where several lines from different vintages within the basin exhibit consistently lower reflectivity as a result of attenuation within the shallow sediments. Future surveys in the Perth Basin might benefit from utilizing infill shots within these specific areas or vertically summing multiple sweeps per source station to potentially improve data quality and subsurface imaging.

# 6 PROCESSED DELIVERABLES

Table 8. 23GSWA-MW1 Processed deliverables

| Item # | File name | Description |
|---|---|---|
| 1. | 23GSWA_MW1_RawGeomFBP-Shots_FFID6-4484_20240605.sgy | Correlated shots with geometry and first break picks |
| 2. | 23GSWA_MW1_RawGeomFBP-Shots_FFID4486-8962_20240605.sgy | |
| 3. | 23GSWA_MW1_RawGeomFBP-Shots_FFID8964-13442_20240605.sgy | |
| 4. | 23GSWA_MW1_RawGeomFBP-Shots_FFID13444-17920_20240605.sgy | |
| 5. | GSWA_MW1_2D_Final_SPS.s | SPS files (text file) |
| 6. | GSWA_MW1_2D_Final_SPS.r | |
| 7. | GSWA_MW1_2D_Final_SPS.x | |
| 8. | 23GSWA_MW1_tomo_picks.pic | First break picks (text file) |
| 9. | Rec_Stat.a_db | Source, receiver and CDP statics files (text file) |
| 10. | Sou_Stat.a_db | |
| 11. | CDP_Stat.a_db | |
| 12. | 23GSWA_MW1_PreMigration-Gathers_part1_20240612_Time@460m.sgy | Pre-processed gathers sorted to CDP and prepared for migration |
| 13. | 23GSWA_MW1_PreMigration-Gathers_part2_20240612_Time@460m.sgy | |
| 14. | 23GSWA_MW1_PreMigration-Gathers_part3_20240612_Time@460m.sgy | |
| 15. | 23GSWA_MW1_PreMigration-Gathers_part4_20240612_Time@460m.sgy | |
| 16. | 23GSWA_MW1_PreSTM-Gathers_Raw_pt1_20240612_Time@460m.sgy | Raw gathers from PreSTM |
| 17. | 23GSWA_MW1_PreSTM-Gathers_Raw_pt2_20240612_Time@460m.sgy | |
| 18. | 23GSWA_MW1_PreSTM-Stk_20sec_Full_Final_20240623_Depth@460m.sgy | 20s record length final PreSTM stack converted to depth |
| 19. | 23GSWA_MW1_PreSTM-Stk_20sec_Full_Final_20240523_Time@460m.sgy | 20s record length final PreSTM stack |
| 20. | 23GSWA_MW1_PreSTM-Stk_20sec_Full_Raw_20240623_Depth@460m.sgy | 20s record length raw PreSTM stack converted to depth |
| 21. | 23GSWA_MW1_PreSTM-Stk_20sec_Full_Raw_20240523_Time@460m.sgy | 20s record length raw PreSTM stack |

| | |
|---|---|
| 22. 23GSWA_MW1_PreSTM-Stk_8sec_Far_Final_20240623_Depth@460m.sgy | 8s record length final PreSTM far angle stack converted to depth |
| 23. 23GSWA_MW1_PreSTM-Stk_8sec_Far_Final_20240523_Time@460m.sgy | 8s record length final PreSTM far angle stack |
| 24. 23GSWA_MW1_PreSTM-Stk_8sec_Far_Raw_20240623_Depth@460m.sgy | 8s record length raw PreSTM far angle stack converted to depth |
| 25. 23GSWA_MW1_PreSTM-Stk_8sec_Far_Raw_20240523_Time@460m.sgy | 8s record length raw PreSTM far angle stack |
| 26. 23GSWA_MW1_PreSTM-Stk_8sec_Full_Final_20240623_Depth@460m.sgy | 8s record length final PreSTM stack converted to depth |
| 27. 23GSWA_MW1_PreSTM-Stk_8sec_Full_Final_20240523_Time@460m.sgy | 8s record length final PreSTM stack |
| 28. 23GSWA_MW1_PreSTM-Stk_8sec_Full_Raw_20240623_Depth@460m.sgy | 8s record length raw PreSTM stack converted to depth |
| 29. 23GSWA_MW1_PreSTM-Stk_8sec_Full_Raw_20240523_Time@460m.sgy | 8s record length raw PreSTM stack |
| 30. 23GSWA_MW1_PreSTM-Stk_8sec_Mid_Final_20240623_Depth@460m.sgy | 8s record length final PreSTM mid angle stack converted to depth |
| 31. 23GSWA_MW1_PreSTM-Stk_8sec_Mid_Final_20240523_Time@460m.sgy | 8s record length final PreSTM mid angle stack |
| 32. 23GSWA_MW1_PreSTM-Stk_8sec_Mid_Raw_20240623_Depth@460m.sgy | 8s record length raw PreSTM mid angle stack converted to depth |
| 33. 23GSWA_MW1_PreSTM-Stk_8sec_Mid_Raw_20240523_Time@460m.sgy | 8s record length raw PreSTM mid angle stack |
| 34. 23GSWA_MW1_PreSTM-Stk_8sec_Near_Final_20240623_Depth@460m.sgy | 8s record length final PreSTM near angle stack converted to depth |
| 35. 23GSWA_MW1_PreSTM-Stk_8sec_Near_Final_20240523_Time@460m.sgy | 8s record length final PreSTM near angle stack |
| 36. 23GSWA_MW1_PreSTM-Stk_8sec_Near_Raw_20240623_Depth@460m.sgy | 8s record length raw PreSTM near angle stack converted to depth |
| 37. 23GSWA_MW1_PreSTM-Stk_8sec_Near_Raw_20240523_Time@460m.sgy | 8s record length raw PreSTM near angle stack |
| 38. 23GSWA_MW1_PreSTM_Velocity_RMST_20240606@460m.sgy | Final PreSTM velocity-RMS |
| 39. 23GSWA_MW1_PreSTM_Velocity_RMST.ascii | Final PreSTM velocity-RMS in ascii format |
| 40. 23GSWA_MW1_PreSTM_Velocity_T-D_conversion_RMST_20240624@460m.sgy | Final PreSTM velocity-RMS converted to depth |
| 41. 23GSWA_MW1_PreSTM_Velocity_T-D_conversion_RMST.ascii | Final PreSTM velocity-RMS converted to depth in ascii format |
| 42. 23GSWA_MW1_PreSTM_Velocity_INTZ_20240606@460m.sgy | Final PreSTM velocity-INT converted to depth |
| 43. 23GSWA_MW1_PreSTM_Velocity_INTZ.ascii | Final PreSTM velocity-INT converted to depth in ascii format |
| 44. 23GSWA_MW1_PreSDM-Gathers_Raw_part1_20240624_Depth@460m.sgy | Raw gathers from PreSDM |
| 45. 23GSWA_MW1_PreSDM-Gathers_Raw_part2_20240624_Depth @460m.sgy | |

| | |
|---|---|
| 46. 23GSWA_MW1_PreSDM-Gathers_Raw_part3_20240624_Depth @460m.sgy | Raw gathers from PreSDM |
| 47. 23GSWA_MW1_PreSDM-Gathers_Raw_part4_20240624_Depth @460m.sgy | |
| 48. 23GSWA_MW1_PreSDM-Stk_Final_20240709_Depth@460m.sgy | 50km record length final PreSDM stack |
| 49. 23GSWA_MW1_PreSDM_Velocity_INTZ_20240709@460m.sgy | Final PreSDM velocity-INT |
| 50. 23GSWA_MW1_TOP-ROCK_Raypaths_20240212_depth@460.sgy | Refraction tomography raypaths |
| 51. 23GSWA_MW1_TOP-ROCK_Velocity_20240212_depth@460.sgy | Refraction tomography velocity model |

Table 9. 23GSWA-MW2 Processed deliverables

| Item # | File name | Description |
|---|---|---|
| 1. | 23GSWA_MW2_RawGeomFBP-Shots_FFID6-2360_20240617.sgy | Correlated shots with geometry and first break picks |
| 2. | 23GSWA_MW2_RawGeomFBP-Shots_FFID2362-4714_20240617.sgy | |
| 3. | 23GSWA_MW2_RawGeomFBP-Shots-FFID4716-7068_20240617.sgy | |
| 4. | 23GSWA_MW2_RawGeomFBP-Shots_FFID7070-9420_20240617.sgy | |
| 5. | GSWA_MW2_2D_Final_SPS.s | SPS files (text file) |
| 6. | GSWA_MW2_2D_Final_SPS.r | |
| 7. | GSWA_MW2_2D_Final_SPS.x | |
| 8. | 23GSWA_MW2_ALL_FBpicks_fromTomo.pic | First break picks (text file) |
| 9. | Rec_Stat.a_db | Source, receiver and CDP statics files (text file) |
| 10. | Sou_Stat.a_db | |
| 11. | CDP_Stat.a_db | |
| 12. | 23GSWA_MW2_PreMigration-Gathers_part1_20240619_Time@370m.sgy | Pre-processed gathers sorted to CDP and prepared for migration |
| 13. | 23GSWA_MW2_PreMigration-Gathers_part2_20240619_Time@370m.sgy | |
| 14. | 23GSWA_MW2_PreMigration-Gathers_part3_20240619_Time@370m.sgy | |
| 15. | 23GSWA_MW2_PreMigration-Gathers_part4_20240619_Time@370m.sgy | |
| 16. | 23GSWA_MW2_PreSTM-Gathers_Raw_pt1_20240620_Time@370m.sgy | Raw gathers from PreSTM |
| 17. | 23GSWA_MW2_PreSTM-Gathers_Raw_pt2_20240620_Time@370m.sgy | |
| 18. | 23GSWA_MW2_PreSTM-Stk_20sec_Full_Final_20240626_Depth@370m.sgy | 20s record length final PreSTM stack converted to depth |
| 19. | 23GSWA_MW2_PreSTM-Stk_20sec_Full_Final_20240626_Time@370m.sgy | 20s record length final PreSTM stack |
| 20. | 23GSWA_MW2_PreSTM-Stk_20sec_Full_Raw_20240626_Depth@370m.sgy | 20s record length raw PreSTM stack converted to depth |
| 21. | 23GSWA_MW2_PreSTM-Stk_20sec_Full_Raw_20240626_Time@370m.sgy | 20s record length raw PreSTM stack |
| 22. | 23GSWA_MW2_PreSTM-Stk_8sec_Far_Final_20240621_Depth@370m.sgy | 8s record length final PreSTM far angle stack converted to depth |

| | | |
|---|---|---|
| 23. | 23GSWA_MW2_PreSTM-Stk_8sec_Far_Final_20240621_Time@370m.sgy | 8s record length final PreSTM far angle stack |
| 24. | 23GSWA_MW2_PreSTM-Stk_8sec_Far_Raw_20240621_Depth@370m.sgy | 8s record length raw PreSTM far angle stack converted to depth |
| 25. | 23GSWA_MW2_PreSTM-Stk_8sec_Far_Raw_20240621_Time@370m.sgy | 8s record length raw PreSTM far angle stack |
| 26. | 23GSWA_MW2_PreSTM-Stk_8sec_Full_Final_20240621_Depth@370m.sgy | 8s record length final PreSTM stack converted to depth |
| 27. | 23GSWA_MW2_PreSTM-Stk_8sec_Full_Final_20240621_Time@370m.sgy | 8s record length final PreSTM stack |
| 28. | 23GSWA_MW2_PreSTM-Stk_8sec_Full_Raw_20240621_Depth@370m.sgy | 8s record length raw PreSTM stack converted to depth |
| 29. | 23GSWA_MW2_PreSTM-Stk_8sec_Full_Raw_20240621_Time@370m.sgy | 8s record length raw PreSTM stack |
| 30. | 23GSWA_MW2_PreSTM-Stk_8sec_Mid_Final_20240621_Depth@370m.sgy | 8s record length final PreSTM mid angle stack converted to depth |
| 31. | 23GSWA_MW2_PreSTM-Stk_8sec_Mid_Final_20240621_Time@370m.sgy | 8s record length final PreSTM mid angle stack |
| 32. | 23GSWA_MW2_PreSTM-Stk_8sec_Mid_Raw_20240621_Depth@370m.sgy | 8s record length raw PreSTM mid angle stack converted to depth |
| 33. | 23GSWA_MW2_PreSTM-Stk_8sec_Mid_Raw_20240621_Time@370m.sgy | 8s record length raw PreSTM mid angle stack |
| 34. | 23GSWA_MW2_PreSTM-Stk_8sec_Near_Final_20240621_Depth@370m.sgy | 8s record length final PreSTM near angle stack converted to depth |
| 35. | 23GSWA_MW2_PreSTM-Stk_8sec_Near_Final_20240621_Time@370m.sgy | 8s record length final PreSTM near angle stack |
| 36. | 23GSWA_MW2_PreSTM-Stk_8sec_Near_Raw_20240621_Depth@370m.sgy | 8s record length raw PreSTM near angle stack converted to depth |
| 37. | 23GSWA_MW2_PreSTM-Stk_8sec_Near_Raw_20240621_Time@370m.sgy | 8s record length raw PreSTM near angle stack |
| 38. | 23GSWA_MW2_PreSTM_Velocity_RMST_20240708_Time@370.ascii | Final PreSTM velocity-RMS in ascii format |
| 39. | 23GSWA_MW2_PreSTM_Velocity_RMST_20240708_Time@370.sgy | Final PreSTM velocity-RMS |
| 40. | 23GSWA_MW2_PreSTM_Velocity_T-D_conversion_RMST_20240711@370m.ascii | Final PreSTM velocity-RMS converted to depth in ascii format |
| 41. | 23GSWA_MW2_PreSTM_Velocity_T-D_conversion_RMST_20240711@370m.sgy | Final PreSTM velocity-RMS converted to depth |
| 42. | 23GSWA_MW2_PreSTM_Velocity_INTZ_20240711@370m.ascii | Final PreSTM velocity-INT converted to depth |
| 43. | 23GSWA_MW2_PreSTM_Velocity_INTZ_20240711@370m.sgy | Final PreSTM velocity-INT converted to depth in ascii format |
| 44. | 23GSWA_MW2_PreSDM-Gathers_Raw_part1_20240719@370m.sgy | Raw gathers from PreSDM |
| 45. | 23GSWA_MW2_PreSDM-Gathers_Raw_part2_2024071@70m.sgy | |
| 46. | 23GSWA_MW2_PreSDM-Gathers_Raw_part3_20240719_Depth@370m.sgy | |

| | |
|---|---|
| 47. 23GSWA_MW2_PreSDM-Gathers_Raw_part4_20240919_Depth@460m.sgy | Raw gathers from PreSDM |
| 48. 23GSWA_MW2_PreSDM-Stk_Final_20240719@370m.sgy | 50km record length final PreSDM stack |
| 49. 23GSWA_MW2_PreSDM_Velocity_INTZ_20240719@370m.sgy | Final PreSDM velocity-INT |
| 50. GSWA_MW2_TOP-ROCK_Raypaths_20240305_depth@370.sgy | Top-rock refraction tomography raypaths |
| 51. GSWA_MW2_TOP-ROCK_Velocity_20240305_depth@370.sgy | Top-rock refraction tomography velocity model |

# 7 REFERENCES

Robinson, E.A., Treitel, S., 2008, Digital Imaging and Deconvolution: The ABCs of Seismic Exploration and Processing.

Sheriff, R. E. and Geldart, L. P., 1995, Exploration Seismology, 2nd Ed., Cambridge Univ. Press, pgs. 49-50

Tanis, M. C., H. Shah, P. A. Watson, M. Harrison, S. Yang, L. Lu, and C. Carvill, 2006, Diving-wave refraction tomography and reflection tomography for velocity model building: 76th Annual International Meeting, SEG, Expanded Abstracts, 3340–3344, http://dx.doi.org/10.1190/1.2370225.

Woodward M. J., D. Nichols, O. Zdraveva, P. Whitfield, and T. Johns, 2008, A decade of tomography: Geophysics, 73, no. 5, VE5–VE11.

Yilmaz, O, 2001, Seismic data analysis: Society of Exploration Geophysicists.

Ziramov, S., Young, C., Kinkela, J., Turner, G. & Urosevic, M. (2023) Pre-stack depth imaging techniques for the delineation of the Carosue Dam gold deposit, Western Australia. Geophysical Prospecting, 00, 1– 19. https://doi.org/10.1111/1365-2478.13314

# 8 APPENDIX

## 8.1 SEGY HEADERS - FIELD SHOTS

See accompanying INOVA trace header specifications document.

INOVA Disk Tape and Tape Image Formats 7D.pdf

## 8.2 SEGY HEADERS - GEOM FBP SHOTS, PRE-MIG GATHERS

Table 10. SEGY headers for Geom, FBP shots and pre-migration gathers

| Header | Byte location | Description |
|---|---|---|
| SOU_STN | 17-20 | Source station |
| CDP | 21-24 | CDP number |
| CDP_FOLD | 33-34 | Fold of CDP |
| OFFSET | 37-40 | Distance from source to receiver |
| REC_ELEV | 41-44 | Surface elevation at receiver |
| SOU_ELEV | 45-48 | Surface elevation at source |
| REC_DATUM | 53-56 | Final datum elevation at receiver (460 m-MW1; 370m-MW2) |
| SOU_DATUM | 57-60 | Final datum elevation at source (460 m MW1; 370m-MW2) |
| SOU_X | 73-76 | Source X coordinate |
| SOU_Y | 77-80 | Source Y coordinate |
| REC_X | 81-84 | Receiver X coordinate |
| REC_Y | 85-88 | Receiver Y coordinate |
| WVEL | 91-92 | Weathering velocity (1000 m/s) |
| SUBWVEL | 93-94 | Sub-weathering velocity |
| SOU_STAT | 99-100 | Source refraction static to final datum |
| REC_STAT | 101-102 | Receiver refraction static to final datum |
| TOT_STAT | 103-104 | Total static applied |
| CDP_X | 181-184 | CDP X coordinate |
| CDP_Y | 185-188 | CDP Y coordinate |
| CDP_STN | 191-194 | CDP station |
| REC_STN | 195-198 | Receiver station |
| CDP_ELEV | 211-212 | Surface elevation of CDP |
| REF_DEPTH | 215-216 | Refractor depth at receiver |
| REF_ELEV | 217-218 | Refractor elevation at receiver |
| REP_VEL | 219-220 | Replacement velocity (5800 m/s) |
| FNL_STAT | 225-226 | Static to move from floating to final datum |
| FB_PICK | 237-240 | First break pick time |

## 8.3 SEGY HEADERS - MIGRATED GATHERS AND STACKS

Table 11. SEGY headers for migrated gathers and stacks

| Header | Byte location | Description |
|---|---|---|
| SOU_STN | 17-20 | Source station |
| CDP | 21-24 | CDP number |
| CDP_FOLD | 33-34 | Fold of CDP |
| OFFSET | 37-40 | Migrated offset bin centre |
| REC_DATUM | 53-56 | Final datum elevation at receiver (460 m MW1; 370m MW2) |
| SOU_DATUM | 57-60 | Final datum elevation at source (460 m MW1; 370m MW2) |
| CDP_X | 73-76 | CDP X coordinate |
| CDP_Y | 77-80 | CDP Y coordinate |
| WVEL | 91-92 | Weathering velocity (1000 m/s) |
| SUBWVEL | 93-94 | Sub-weathering velocity |
| CDP_X | 181-184 | CDP X coordinate |
| CDP_Y | 185-188 | CDP Y coordinate |
| CDP_STN | 191-194 | CDP station |
| REC_STN | 195-198 | Receiver station |
| CDP_ELEV | 211-212 | Surface elevation of CDP |
| REF_ELEV | 217-218 | Refractor elevation at receiver |
| REP_VEL | 219-220 | Replacement velocity (5800 m/s) |
| TOT_STAT | 223-224 | Total static applied |
| FNL_STAT | 225-226 | Static to move from floating to final datum |

## 8.4 ACCOMPANYING TEST REPORTS AND WEEKLY UPDATES

Table 12. 23GSWA-MW1 Test reports and weekly updates

| Item # | File name |
|---|---|
| 1. | 20240109_GSWA_MW1_Processing_update.pdf |
| 2. | 20240206_GSWA_MW1_Preliminary_Tomography.pdf |
| 3. | 20240212_GSWA_MW1_Final_Tomography.pdf |
| 4. | 20240312_GSWA_MW1_Processing_update.pdf |
| 5. | 20240326_GSWA_MW1_Processing_update.pdf |
| 6. | 20240409_GSWA_MW1_Processing_update.pdf |
| 7. | 20240416_GSWA_MW1_Processing_update.pdf |
| 8. | 20240423_GSWA_MW1_Processing_update.pdf |
| 9. | 20240507_GSWA_MW1_Processing_update.pdf |
| 10. | 20240513_GSWA_MW1_Processing_update.pdf |
| 11. | 20240514_GSWA_MW1_PSDM_imaging_update.pdf |
| 12. | 20240521_GSWA_MW1_Processing_update.pdf |
| 13. | 20240521_GSWA_MW1_PSDM_imaging_update.pdf |
| 14. | 20240528_GSWA_MW1_PSDM_imaging_update.pdf |
| 15. | INOVA Disk Tape and Tape Image Formats 7D.pdf |

Table 13. 23GSWA-MW2 Test reports and weekly updates

| Item # | File name |
|---|---|
| 1. | 20240305_GSWA_MW2_Final_Tomography.pdf |
| 2. | 20240430_GSWA_MW2_Processing_update.pdf |
| 3. | 20240507_GSWA_MW2_Processing_update.pdf |
| 4. | 20240514_GSWA_MW2_Processing_update.pdf |
| 5. | 20240528_GSWA_MW2_Processing_update_combined.pdf |
| 6. | 20240604_GSWA_MW2_Processing_update.pdf |
| 7. | 20240611_GSWA_MW2_Processing_update.pdf |
| 8. | 20240617_GSWA_MW1_MW2_DepthImaging_update.pdf |
| 9. | 20240618_GSWA_MW2_Processing_update.pdf |
| 10. | 20240625_GSWA_MW1_MW2_Processing_update.pdf |
| 11. | 20240702_GSWA_MW2_Processing_update.pdf |
| 12. | 20240709_GSWA_MW2_Processing_update.pdf |
| 13. | 20240716_GSWA_MW2_Processing_update.pdf |
| 14. | 20240723_GSWA_MW2_Processing_update.pdf |
| 15. | INOVA Disk Tape and Tape Image Formats 7D.pdf |

## 8.5 SEISOMICS

**Title:** Revealing Geological Details in Hard Rock Seismic Volumes using Medical Imaging Technology

**Abstract:** We present "Seisomics", a machine-learning workflow to segment and classify seismic imaging data into domains of similar statistical texture. This approach has been adapted from medical imaging; customizing the image feature sets from the Image Biomarker Standardisation Initiative (IBSI) V1 for application on 3D and 2D seismic datasets. The method aims to "discriminate potentially meaningful differences in imaging which are not readily apparent to the human eye". This is first performed by computing a textural and co-located petrophysical attributes and then applying classification algorithms. This segments the imaging volume into regions. Where dimensionality reduction algorithms can be applied to improve classification with higher dimensionality datasets. This method aims to reveal high-resolution geological details in the near-surface, imaging subtle transitions in geochemistry or geology.

**Co-Authors:**

1. Dr. Andrew M. Pethick*, HiSeis, A.Pethick@hiseis.com

2. Mrs. Sian Bright, HiSeis, S.Bright@hiseis.com

3. Mr. Jeremy Smith, HiSeis, J.Smith@hiseis.com

*Address For all Authors: HiSeis Pty Ltd, 140 Hay Street, Subiaco, Western Australia*

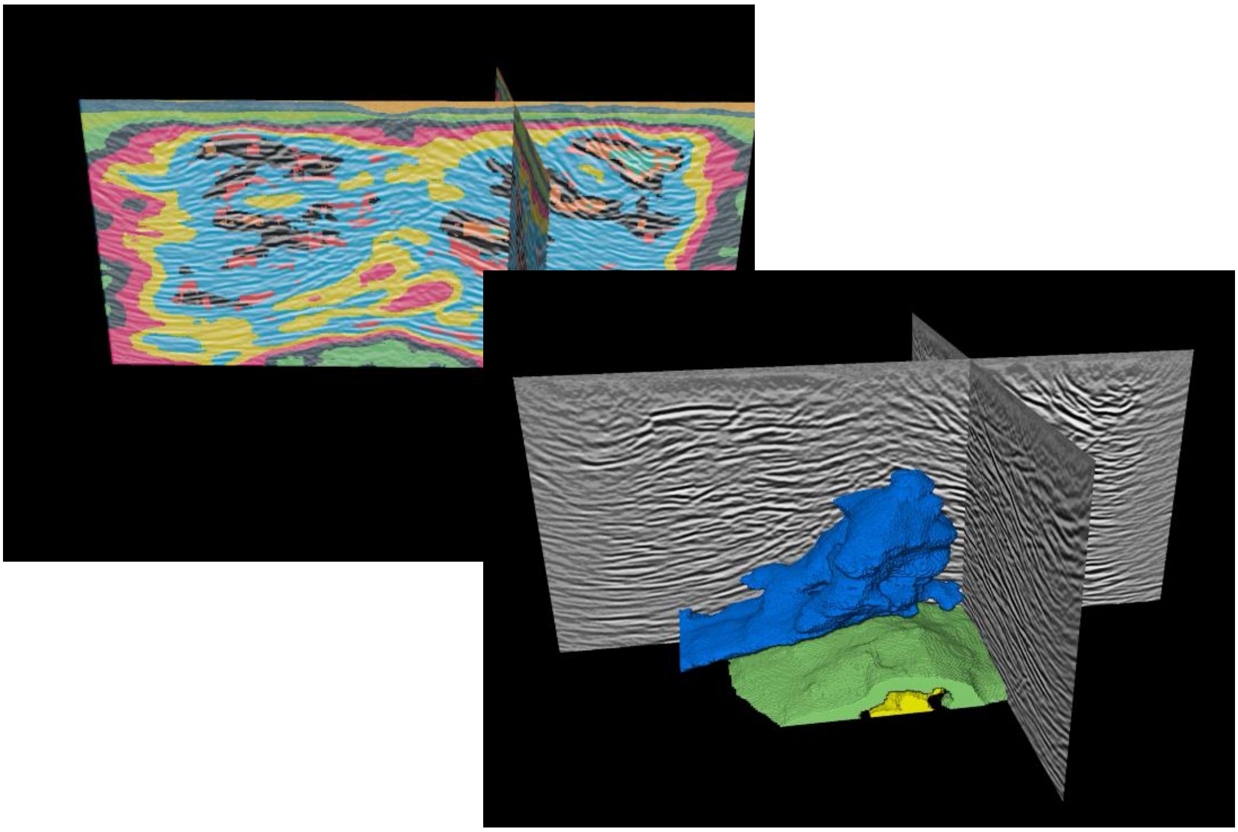

HiSeis

**hiseis.com**

140 Hay Street, Subiaco WA 6008
+61 8 9470 9866